Trisomy 21 drives production of neurotoxic tryptophan catabolites via the interferon-inducible kynurenine pathway

Authors:

Rani K. Powers[1,2,3#], Kelly D. Sullivan[1,3#], Rachel Culp-Hill[4], Michael P. Ludwig[1], Keith P. Smith[1], Katherine A. Waugh[1], Ross Minter[1], Kathryn D. Tuttle[1], Angela L. Rachubinski[1], Ross E. Granrath[1], Rebecca B. Wilkerson[4], Angelo D'Alessandro[1,4], James C. Costello[2,3,*] & Joaquin M. Espinosa[1,3,5*]

Affiliations:

[1]Linda Crnic Institute for Down Syndrome, University of Colorado Anschutz Medical Campus, Aurora, CO, USA

[2]Computational Bioscience Program, University of Colorado Anschutz Medical Campus, Aurora, CO, USA

[3]Department of Pharmacology, University of Colorado Anschutz Medical Campus, Aurora, CO, USA

[4]Department of Biochemistry and Molecular Genetics, University of Colorado Anschutz Medical Campus, Aurora, CO, USA

[5]Department of Molecular, Cellular and Developmental Biology, University of Colorado Boulder, Boulder, CO, USA

[#]These authors contributed equally to this work

[*]Corresponding Authors:

James C. Costello: james.costello@ucdenver.edu,Joaquin M. Espinosa: joaquin.espinosa@ucdenver.edu

ABSTRACT.

Trisomy 21 (T21) causes the condition known as Down syndrome (DS), with clear impacts on brain development and function. In a previous paper (Sullivan, 2016) we showed that T21 consistently activates the interferon (IFN) response, but the contribution of IFN hyperactivity to DS phenotypes awaits elucidation. Here, we report the results of a large plasma metabolomics study, showing that T21 disrupts tryptophan catabolism toward increased production of kynurenine (KYN) and its neurotoxic derivative quinolinic acid. We also show that stimulation of IFN signaling leads to tryptophan depletion, over-production of KYN, and super-induction of IDO1, the rate-limiting enzyme in the KYN pathway, in human cells with T21 and a mouse model of DS. Finally, cytokine profiling revealed a positive correlation between circulating levels of IFNα and KYN dysregulation in people with DS. Altogether, these results reveal a mechanism by which IFN hyperactivity could drive cognitive deficits and neurodegeneration in DS.

INTRODUCTION.

Down syndrome (DS) is caused by triplication of chromosome 21 (trisomy 21, T21), which occurs in approximately 1 in 700 live births, representing the most common chromosomal abnormality in the human population (1). T21 impacts multiple organ systems during development and causes an altered disease spectrum in people with DS, significantly increasing their risk of developing Alzheimer's disease (AD), leukemia, and numerous autoimmune conditions (1-7), while protecting them from solid malignancies (8, 9). However, DS-associated phenotypes are highly variable among individuals with DS, even for conserved phenotypes such as cognitive impairment and predisposition to early onset AD (2, 10). Therefore, a deeper understanding of the mechanisms driving such phenotypic variation could illuminate not only mechanisms of pathology, but also opportunities for diagnostics and therapeutic strategies to serve this special population.

In order to identify molecular pathways that could contribute to both the altered disease spectrum experienced by the population with DS as well as the inter-individual variation among phenotypes, our group previously analyzed transcriptomes (11) and circulating proteomes (12) from several cohorts of individuals with DS compared to euploid individuals (D21, controls). These efforts revealed that multiple cell types from people with T21 show transcriptional signatures indicative of constitutive activation of the interferon (IFN) response (11), which could be explained by the fact that four of the six IFN receptors are encoded on chr21 (13). Furthermore, plasma proteomics analyses demonstrated that people with DS show signs of chronic autoinflammation (12), including elevated levels of potent inflammatory cytokines with known ties to IFN signaling (e.g. IL-6, TNF-α). However, it remains to be defined how this obvious immune dysregulation contributes to highly variable DS-associated phenotypes, including the diverse neurological manifestations of T21. To gain further insight into this area, we investigated metabolic changes caused by T21 in the plasma of people with DS.

Here, we report the results of the largest plasma metabolomics study of individuals with DS to date using untargeted, highly sensitive liquid chromatography mass spectrometry (LC-MS) technology. We discovered dysregulation of a number of inflammation-associated metabolites, such as succinate and 2-hydroxyglutarate (14, 15), in individuals with DS. However, most prominent among the dysregulated metabolites were those related to tryptophan catabolism. Specifically, people with DS showed highly statistically significant upregulation of kynurenine (KYN) and its neurotoxic derivative quinolinic acid (QA) (16). Using an unbiased, machine learning approach to build a predictive metabolic signature of T21, we found that select metabolites in the tryptophan pathway, along with other inflammation-associated metabolites, can accurately distinguish plasma from individuals with DS from euploid controls. Using cell-based metabolic flux assays, we found that IFN-α stimulation leads to profound depletion of tryptophan in T21 cells, along with markedly increased production of KYN, which could be explained by overexpression of IDO1, the rate-limiting enzyme in the KYN pathway and a known interferon stimulated gene (17). We found that a mouse model of DS that includes triplication of the IFN receptor gene cluster, *Dp(16)1/Yey*, has increased levels of KYN relative to wild type littermates, and produces more KYN when injected with the IFN-stimulating molecule poly(I:C). Given the well-established roles of KYN dysregulation on a wide range of neurological conditions (18-20), our results suggest that IFN-dependent activation of the KYN pathway could contribute to key neurological phenotypes in DS.

RESULTS.

Trisomy 21 causes consistent changes in plasma metabolite abundance.

In order to identify metabolic pathways that are consistently dysregulated by T21, we collected plasma samples from two fully independent cohorts: the Translational Nexus Clinical Data Registry and Biobank (referred hereto as Cohort 1), and the Crnic Institute's Human Trisome Project (www.trisome.org, NCT02864108, referred hereto as the Cohort 2). Cohort 1 included 49 individuals with T21 and 49 euploid (D21) individuals, while Cohort 2 consisted of 30 T21 and 41 D21. The breakdown of patients according to age and sex are reported in **Table 1**. While the Cohort 1 is balanced for karyotype but imbalanced for age, Cohort 2 is more age-balanced, with a bias towards females in both D21 and T21 groups. When the two cohorts are combined, age, sex, and karyotype are more evenly distributed, which prompted us to analyze the cohorts both individually and in combination. Because the variables of age, sex, and cohort-specific features (e.g. protocol for sample collection, processing and storage), can influence metabolite abundance and/or detection, we accounted for these variables when determining the impact of karyotype as described below.

To determine metabolite abundance, we performed untargeted, LC-MS metabolomics on plasma from each cohort. The combined analysis workflow is outlined in **Figure 1 – figure supplement 1A** with details available in the **Materials and Methods.** This approach led to the identification of 91 high-confidence metabolites detected in both cohorts. To identify those that are consistently differentially abundant between people with and without DS, we employed a robust linear model-fitting approach that accounted for age, sex, and cohort (21). We arrived at this model after evaluating each of these variables in the cohorts individually, as well as in combination. Using the 91-metabolite panel, we first evaluated the impact of age and sex within each cohort. We fit linear models and compared the results within Cohort 1, where we included or excluded the variables age and sex directly in the model (**Figure 1 – figure supplement 1B**). We found that taking age and sex into account directly impacted the differential abundance statistics when comparing T21 to D21 individuals; this result was expected given the differences in age and sex seen in Cohort 1. We performed the same comparison within Cohort 2 (**Figure 1 – figure supplement 1C**) and found similar results, although age and sex had less of an impact as Cohort 2 is more balanced. The differences observed between cohorts motivated us to evaluate the impact of a combined cohort analysis, with the goal of mitigating the biases within each of the individual cohorts and increasing our statistical power with a greater number of individuals.

Integrating data across cohorts required us to evaluate the impact of each cohort as a batch effect. Indeed, we observed strong differences in the distributions of metabolite abundances between cohorts (**Figure 1 – figure supplement 2A**). By using the same linear model fit, while additionally including the cohort as the batch covariate in the model, thus accounting for age, sex, and cohort, the distributions of metabolite abundance became overlapping and comparable (**Figure 1 – figure supplement 2B**). We confirmed the impact of the cohorts as a model covariate using principal components analysis (PCA), showing that the first principal component can explain the variation seen between cohorts (**Figure 1 – figure supplement 2C**). After accounting for patient cohort, along with age and sex in the model, the first two principal components no longer account for variation that can be attributed to the modeled covariates (**Figure 1 – figure supplement 2D**), indicating that

the two cohorts can be combined to find metabolite changes that are attributable to karyotype rather than systematic effects associated with age, sex, and cohort-specific variables.

When the combined total of samples in the two cohorts were analyzed for the 91 metabolites using the linear model fit including age, sex, and cohort covariate, we identified 16 metabolites that are significantly differentially abundant according to a Benjamini-Hochberg adjusted p-value cut-off of 0.01 (**Figure 1A, Supplemental File 1A**). Of these, seven were less abundant in the plasma of individuals with T21 and nine were more abundant.

Among the significantly depleted metabolites are the amino acids L-serine and L-tyrosine, consistent with earlier reports (22, 23) (**Figure 1A-B**). Depletion of L-homocysteine (**Figure 1A-B**), which has also been previously observed in people with DS (24), could be attributed to the localization of the cystathionine-beta-synthase gene (*CBS*) on chr21. Among upregulated metabolites we observed succinate and 2-hydroxyglutarate, two metabolites related to the TCA cycle (**Figure 1A-B**). Elevated succinate levels have been previously reported in people with DS and interpreted as a sign of mitochondrial dysfunction (23), but succinate upregulation is also an established marker of inflammation (14). Other upregulated metabolites include the antioxidant molecules dehydroascorbate and mannitol (**Figure 1A-B**) (25, 26). In order to identify metabolic pathways that were systematically dysregulated in individuals with T21, we performed an unbiased pathway enrichment analysis. We tested a total of 52 KEGG pathways (27) that had at least 5 metabolites included in our 91 metabolites (**Supplemental File 1B**). Using a hypergeometric test, the most significantly enriched pathway was Tryptophan Metabolism (p-value = 0.002, adj. p = 0.096). In fact, of the 11 tryptophan catabolic metabolites annotated in this pathway and detected in our analysis, five are differentially abundant: KYN, QA and 5-hydroxyindoleacetate are upregulated, while indole and indole-3-acetaldehyde are downregulated (**Figure 1C**). As noted later, depletion of L-serine could also be related to dysregulated tryptophan metabolism (**Figure 1A-B,** see later **Figure 3 – figure supplement 2**).

A signature of tryptophan catabolites and inflammatory metabolites accurately stratifies plasma samples from individuals with trisomy 21.

Next, we employed a machine-learning approach to investigate whether metabolites identified with our platform could be used to stratify plasma samples provided from individuals with or without DS (see **Materials and Methods** for details). As a baseline for comparison, we established the predictive power of each of the 16 differentially abundant metabolites (**Figure 2A**). To achieve this, we used metabolite abundance as a predictor of T21 that we evaluated using receiver operatic characteristic curves (ROC), which compares the true positive rates (TPR) to false positive rate (FPR). Interestingly, QA had the most predictive value (AUC = 0.73) (**Figure 2A**). Next, to determine the predictive potential of multivariate plasma metabolic profiles to distinguish T21 from D21, we prioritized metabolites based on their predictive value using a lasso regression feature selection approach (28). To achieve this, we trained 10,000 independent, 5-fold cross-validated lasso regression models on the combined data set of both cohorts to identify metabolites that were consistently selected in models with high predictive value. The coefficients of an individual metabolite reflect the metabolite's weight in that model, thus we selected the metabolites with the greatest average coefficient weights that were consistently selected in

over 80% of the trained models with an accuracy > 0.9. This analysis yielded 11 metabolites, of which eight had positive model coefficients and three had negative model coefficients (**Figure 2B**). These 11 metabolites included seven of the 16 most differentially abundant metabolites and an additional four from the remaining 75 metabolites in our analysis, demonstrating that this approach is not simply selecting the most differentially abundant metabolites, but rather the model is selecting the groups of metabolites that together provide the strongest predictive power. The most frequently selected metabolites included three members of the tryptophan metabolism pathway: QA, KYN, and 3-indole-acetaldehyde (**Figure 2B**). Of note, these three metabolites were selected in 100% of models with > 90% accuracy, while acyl-C5:1 had the largest median positive model coefficient. Next, we evaluated the predictive power across the combined Nexus and HTP cohort using the selected most predictive 11 metabolites. We performed a bootstrapped analysis using a lasso regression to benchmark model performance. We split the combined cohort to train the model on 80% of the participants (randomly selected) and tested performance using the held-out 20%. We repeated this process for 10,000 iterations and found an average model performance of AUC=0.88 with a 95% confidence interval of [0.76, 0.97] (**Figure 2C**).

These results demonstrate that there is strong predictive power within a small group of plasma metabolites for stratifying T21 individuals from D21 individuals. Also, using an independent methodology, these results confirm that differential tryptophan metabolism is a major contributor to the distinguishing metabolic profile of people with DS, which prompted us to investigate this result in more depth.

Trisomy 21 induces the kynurenine pathway.

In vertebrate cells, there are three major catabolic pathways for tryptophan, leading to the production of serotonin, KYN, or indole (**Figure 3**). There is a 10% decrease in L-tryptophan levels in individuals with T21, though it does not rise to the level of significance (p = 0.05, adjusted p = 0.12) (**Figure 3**, **Supplemental File 1A**). There is also an approximately 10% decrease in serotonin, which is not significantly different between T21 and D21. However, 5-hydroxyindoleacetate (5-HIA), a breakdown product of serotonin, is significantly elevated in the group with T21 (adjusted p = 3e-3) (**Figure 3**). Conversion of tryptophan to KYN represents a major pathway for catabolism of ingested tryptophan, accounting for removal of up to 99% of this amino acid that is not used in protein synthesis (29). Remarkably, KYN itself and the neurotoxic downstream product QA, are significantly elevated in people with DS (**Figure 3**). In contrast, picolinic acid (PA), a neuroprotective derivative of KYN, is not different between the two groups (**Figure 3**). Kynurenic acid (KA), another neuroprotective metabolite in the pathway, was detected only in Cohort 2 and was not affected by karyotype (**Figure 3 – figure supplement 1A**). Accordingly, the KYN/tryptophan, QA/PA, and QA/KA ratios are all significantly higher in people with DS (**Figure 3 – figure supplement 1B-D**). Notably, indole and its derivative indole-3-acetaldehyde, both of which are significantly decreased in the T21 group (**Figure 3**), are metabolites produced from tryptophan by tryptophanase-expressing gastrointestinal microbiota (30, 31). Interestingly, indole can also be employed by the gut microbiota to synthesize tryptophan in a reaction that consumes L-serine (31), an amino acid that is significantly depleted in the plasma of people with DS (**Figure 3 – figure supplement 2**). Thus, lower levels of

indole and L-serine could be interpreted as a sign of increased tryptophan biosynthesis by the gut microbiome to sustain levels of this essential amino acid when it is shunted into the KYN pathway in people with DS.

Altogether, our results indicate that a major metabolic impact of trisomy 21 is a dysregulation of tryptophan catabolism toward increased production of the neurotoxic metabolites in the KYN pathway. This is an important result, because activation of the KYN pathway has been implicated in myriad neurological and neurodegenerative disorders. Repeatedly, elevations in the KYN/tryptophan ratio, QA/PA, and/or QA/KA ratios have been linked to the development of neurological conditions such as Alzheimer's disease (32-35), Huntington's disease (36, 37), AIDS/HIV-associated neurocognitive disorder (38-40), Parkinson's disease (41), amyotrophic lateral sclerosis (42, 43), and multiple sclerosis (44, 45).

Trisomy 21 sensitizes cells to super-induction of the KYN pathway upon IFN stimulation.

In order to further investigate the mechanism of KYN dysregulation in DS, we employed cell-based metabolic flux experiments using isotope-labelled tryptophan on a panel of age- and sex-matched skin fibroblasts with and without T21. Of note, the rate-limiting step in the KYN pathway is the conversion of L-tryptophan into N-formyl-kynurenine, a reaction catalyzed by the tryptophan 2,3 dioxygenase 2 (*TDO2*) enzyme in the liver or the indoleamine 2,3 dioxygenases 1 and 2 (*IDO1-2*) enzymes elsewhere (17). Importantly, *IDO1* is a well-recognized IFN-stimulated gene (ISG) whose expression can be induced by Type I (α/ β) and Type II (γ) IFN ligands (46-50). Given our previous finding that T21 fibroblasts are hypersensitive to IFN-α, β, and γ stimulation (11), we performed these experiments before and after IFN-α stimulation. Remarkably, IFN-α stimulation produced a significant, time-dependent depletion of tryptophan in T21 cells, but not supernatant (**Figure 4A, Figure 4 - figure supplement 1A, Supplemental File 1C**), concurrent with a significant increase in KYN levels in the supernatant, but not cells (**Figure 4B, Figure 4 - figure supplement 1B**). The restriction of isotope-labeled tryptophan depletion to the cells is likely due to isotope-labeled tryptophan being far in excess in the supernatant. Accordingly, the KYN/tryptophan ratio was significantly elevated upon IFN-α stimulation only in T21 supernatants and cells (**Figure 4 - figure supplement 1C,D**), and most prominent between KYN in the supernatant and tryptophan in the cells, consistent with consumption of intracellular tryptophan and subsequent secretion of KYN (**Figure 4C**). Matched Western blot analysis showed that T21 fibroblasts display stronger induction of STAT1 phosphorylation (a transcription factor driving IDO1 transcription) and subsequent IDO1 expression at the protein level, than in D21 cells (**Figure 4D**). In fact, after 24 hours of IFN-α treatment, all three T21 cell lines employed in the metabolic flux assay expressed much higher levels of IDO1 relative to their diploid counterparts (**Figure 4E**).

Together, these results provide a mechanistic explanation for the observed dysregulated levels of tryptophan catabolites in plasma of people with DS, whereby T21, likely via overexpression of the four IFNRs encoded on chr21, would provoke a systemic hyper-sensitivity to IDO1 induction in response to IFN signaling.

Tryptophan catabolism is selectively disrupted in the *Dp(16)1/Yey* mouse model of DS.

To test the impact of various groups of genes encoded on human chr21 on tryptophan metabolism, we employed three cytogenetically distinct mouse strains carrying segmental duplications syntenic to human chr21

(51): *Dp(10)1/Yey* (Dp10), *Dp(16)1/Yey* (Dp16), and *Dp(17)1/Yey* (Dp17), which have triplication of ~35 genes from mouse chr10, ~120 genes from chr16, and ~20 genes from chr17, respectively, and compared them to wild type C5Bl/6 mice (WT). We prepared plasma samples from age- and sex-matched cohorts comprised of these strains and measured kynurenine using LC-MS. Interestingly, we found that the only strain with significantly increased plasma KYN levels relative to WT mice was the Dp16 model, which is not only the largest segmental duplication, but the one harboring the four IFN receptors homologous to those found on human chr21: *Ifnar1*, *Ifnar2*, *Ifngr2*, and, *Il10rb* (**Figure 5A**). Furthermore, we and others have previously shown that not only are the IFN receptors overexpressed in this model, but downstream IFN signaling is chronically activated on numerous tissues including blood and brain (11, 52). Therefore, we focused exclusively on this model in subsequent studies. To determine the impact of further stimulation of IFN signaling on altered tryptophan catabolism in Dp16 mice, we chronically injected age and sex-matched Dp16 and WT mice with the synthetic dsRNA polyinosinic:policytidylic acid (poly(I:C)) or a sham control using an established protocol (53), and collected plasma samples. Poly(I:C) activates pattern recognition receptors including TLR3, RIG-I/MDA5, and PKR, with subsequent upregulation of Type I IFN production and concomitant downstream signaling (54). Metabolomic analysis of WT mice revealed modestly increased levels of KYN in poly(I:C)-treated-group relative to the Sham-injected control group; however, only the Dp16 mice displayed statistically significantly higher levels of KYN when injected with poly(I:C) (**Figure 5B**).

These results are consistent with a gene-specific component to dysregulation of the KYN pathway and further implicate triplication of the IFN receptor locus as a key contributor. Moreover, they demonstrate the heightened sensitivity of an IFN receptor-triplicated model to KYN production in response to IFN stimulation at the organismal level.

Kynurenine dysregulation positively correlates with circulating levels of IFNα and downstream cytokines.

Recently, we reported the results of the largest plasma proteomics study of people with DS to date (12), which revealed that T21 causes changes in the circulating proteome indicative of chronic autoinflammation, including elevated levels of many cytokines acting downstream of IFN signaling. Hence, we decided to test whether there was a correlation between inflammatory markers and KYN dysregulation. Toward this end, we measured a panel of 38 cytokines using a Mesoscale Discovery (MSD) assay in 37 participants in Cohort 2, 18 of them with DS, the other 19 being mostly age- and sex-matched typical controls. We calculated Spearman's correlation between specific metabolites of interest versus all cytokines measured. Strikingly, the top cytokine positively correlated with KYN levels among those with DS was IFN-α2a (ρ = 0.67, **Figure 6A**). In fact, most of the cytokines positively correlated with KYN levels (ρ > 0.3) are known to be induced by IFN signaling in various settings, such as MCP-1, IL-33, IL-31, IP-10, IL-8, MIP-1α, MCP-4, IL-27, and TNF-α (55-69). In most cases, the positive correlation was unique to people with DS (see for example IFN-α2a, MCP-1, **Figure 6B, C**). A similar result was obtained for the QA correlation analysis, with the top positively correlated markers being MCP-1 (CCL2) and MCP-4 (CCL13), two known IFN-inducible monocyte chemotactic proteins (61, 65) (**Figure 6D**). Once again, most positively correlated cytokines (ρ > 0.3) are known to act downstream of IFN signaling (55-

69). As for KYN, the correlations were unique to or more pronounced in people with DS (see for example MCP1 and MCP4 (**Figure 6E,F**)).

Altogether, the combination of correlative studies in plasma samples and cause-effect relationships using cell-based assays support the notion that dysregulation of tryptophan metabolism in DS is driven by hyperactive IFN signaling downstream of T21.

DISCUSSION.

The developmental and clinical impacts of T21 in the population with DS are highly variable, with a large number of co-morbidities showing increased prevalence in this population relative to typical people. Despite many research efforts in this area, little is known about the molecular pathways that drive the various co-morbidities common in DS. Clearly, identification of these pathways would facilitate the design of diagnostic and therapeutic strategies to serve this at-risk population via precision medicine approaches. An obvious impact of these approaches would be in the management of diverse neurological conditions showing increased prevalence in this population, including, but not restricted to, early onset AD (3, 10, 70, 71), epilepsy (72), depression (73), and autism (74, 75). Our results point to dysregulation of the KYN pathway as a potential contributing factor to the development of these conditions in people with DS, with obvious diagnostics and therapeutic implications as described below.

People with DS constitute the largest population with a strong predisposition to AD, which is attributed to the fact that the *APP* gene is located on chr21 (3, 70, 71, 76), and that *APP* duplication causes familial early onset AD in the typical population (77). By age 40, virtually all individuals with DS present the brain pathology of AD; however, the age of dementia diagnoses is highly variable, with some individuals being diagnosed in their 30's, while others remain dementia-free in their 70's (78, 79). Therefore, the population with T21 provides a unique opportunity to identify mechanisms that either accelerate or delay AD development. The results in this report, when integrated with a significant body of literature, support the existence of an IFN→IDO1→KYN signaling pathway that could accelerate AD onset and progression in people with DS. First, it is clear that people with DS display chronic immune dysregulation with clear ties to IFN signaling. We recently reported a comprehensive analysis of the circulating proteome of people with DS (12), which revealed clear signs of immune dysregulation across the lifespan. These, and other efforts in the field (80), have identified a core set of inflammatory markers elevated in people with DS, including MCP-1, IL-6, TNF-α and IL-1β, all of which are known to be induced by IFN signaling and whose levels are both elevated in typical people with AD and positively associated with AD progression (55, 81-83). Here, we show that circulating levels of IFN-α2a and MCP-1 positively correlate with dysregulation of the KYN pathway (**Figure 5**), which has been repeatedly associated with AD development (see below) (32, 35, 84, 85). Second, T21 consistently activates the IFN transcriptional response across diverse cell types, including circulating immune cells (11), which is likely due to the fact that four of the six IFNRs are encoded on chr21 (86). Accordingly, T21 cells are hypersensitive to IFN ligands and show significant overexpression of ISGs (11, 86-88), including IDO1, the rate limiting enzyme in the KYN pathway. Pioneering work by Dr. Leonard Maroun and colleagues showed that reduction of IFN signaling in the

early Ts16 mouse model of DS, with either anti-IFN antibodies or by crossbreeding with a strain lacking two *IFNR*s, improved embryonic development and increased survival of cortical neurons *in vitro* (89-91). Additionally, connections between IFN signaling and T21 were established as early as in the 1970s (13, 92-94), but never explored fully. Third, IFN signaling is likely to promote neuropathology and AD progression both upstream and downstream of amyloid deposition. IFN signaling was shown to enhance APP expression and processing into the pathological amyloid peptide, $A\beta_{1-42}$, leading to increased amyloid plaque formation (95, 96). Furthermore, in mouse models of AD, IFN signaling was shown to mediate neuroinflammation, neuronal cell death, and cognitive decline downstream of amyloid plaque formation (96-99). Finally, the KYN pathway has been consistently implicated in AD progression. Multiple studies have reported elevated levels of metabolites in the KYN pathway in people with AD, and, in many of these studies, KYN dysregulation has been positively correlated with AD progression (35, 84, 85, 100-105). Furthermore, IDO1 inhibition reverses AD pathology driven by injection of $A\beta_{1-42}$ in mice (106) and in an early transgenic mouse model of AD (107). Based on these observations, we hypothesize here that those individuals with DS showing the strongest degree of dysregulation in the IFN→IDO1→KYN pathway will also display earlier onset and faster progression of AD. Clearly, testing this hypothesis will require a significant effort, including a multi-dimensional, longitudinal analysis of IFN signaling, KYN dysregulation, and various metrics of the AD pathological cascade.

Beyond AD, it is possible that KYN dysregulation is a driver of other neuropathologies more prevalent in DS, such as epilepsy/infantile spasms/seizures, depression, and autism (72-75). KYN and QA were shown to promote seizures in mice, rats, and frogs (108-111), and QA was found to be elevated in mouse models of epilepsy (112), leading to the characterization of QA as an 'endogenous convulsant' with a pathogenic role in seizure disorders (113). The role of tryptophan catabolism in depression is undisputed (114), with a prominent role for serotonin depletion as a causative event, leading to the widespread therapeutic use of selective serotonin reuptake inhibitors (SSRIs). Importantly, activation of the KYN pathway shunts tryptophan away from serotonin synthesis, causing serotonin depletion, which led Lapin and others to propose the 'kynurenine hypothesis' of depression (115). The discovery of the neurotropic activities of KYN and its derivatives indicated that induction of the KYN pathway could not only drive serotonin deficiency, but also promote depression-associated anxiety, psychosis, and cognitive decline (116). Notably, it has been amply documented that therapeutic administration of IFN-α can induce depression (117-119). During therapeutic use of IFN-α for the treatment of hepatitis C, high tryptophan breakdown was associated with depression-like symptoms during the course of treatment, leading Wichers et al. to propose that IDO1 induction (and consequent neurotoxicity) was the principal pathophysiological mechanism (50, 120). Regarding autism, independent cohort studies have documented dysregulation of KYN metabolism in patients diagnosed with autism spectrum disorder (ASD) (121, 122), as demonstrated by increased KYN/KA ratios (122) and elevated levels of QA (121), adding further evidence to the growing notion of neuroinflammatory processes in the etiology of ASD (123).

In addition to the recognized neurological conditions discussed above, KYN dysregulation could contribute to the cognitive deficits associated with DS. The acute effects of KYN metabolites, QA in particular, on cognitive function are well documented (16, 124). QA is a potent neurotoxin that acts as an excitotoxic *agonist*

of NMDA receptors, and which may also exert toxicity via oxidative stress (9). Importantly, dysregulation of the KYN pathway in DS could explain a large body of work showing beneficial effects of memantine, an NMDA *antagonist* that protects from QA-mediated neurotoxicity (10-13), as well as anti-oxidants such as vitamin E, in various animal models of DS (125-129). Of note, memantine is an approved drug for the treatment of AD, which is currently being tested in a follow-up Phase II clinical trial to improve cognition in young adults with DS (NCT02304302). The initial pilot trial showed benefits on a subset of neurocognitive measures (130). A second independent trial, which focused on adults 40 years and older, showed no effects in any of the endpoints (131). However, we posit here that the limited therapeutic effect of this drug is due to its action at a very downstream step in the pathway, and that inhibitors of IDO1 (107, 132), kynurenine-3-monooxygenase (KMO) (133), and IFN signaling (e.g. JAK inhibitors, decoy IFNR receptors) (134, 135) should be considered. Even if memantine is pursued further, we suggest that its use should be accompanied by an assessment of the degree of KYN dysregulation in those receiving the drug. In principle, memantine should have no benefits for individuals with DS who display normal levels of QA.

Finally, it is important to note that the KYN pathway plays major roles in immune control. KYN is a potent immunosuppressive metabolite promoting 'immune privilege' in tissues such as the brain, testes, and gut, but which is also exploited by some tumor types to evade immune surveillance (17, 136). KYN upregulation in people with DS may affect key cell types involved in autoimmunity, such as regulatory T cells (17, 136), and it may represent an immunosuppressive negative feedback mechanism downstream of chronic IFN signaling (46-49, 137). Given that people with DS are highly predisposed to myriad autoimmune disorders, and that *Pneumonia* lung infections are the top cause of death in people with DS (138), our results justify future investigations to define the role of KYN dysregulation in multiple common co-morbidities in DS.

Materials and Methods

Human cohorts and sample collection

All human subjects in this study were consented according to Colorado Multiple Institutional Review Board (COMIRB)-approved protocols. Written informed consent was obtained from parents or guardians of participants under the age of 18, and assent was obtained from participants over the age of 7 who were cognitively able to assent. Deidentified plasma samples were obtained from the Translational Nexus Clinical Data Registry and Biobank (University of Colorado Anschutz Medical Campus, COMIRB #08-1276) for 49 individuals with DS and 49 controls without DS. Additionally, plasma samples for 31 individuals with DS and 42 controls were obtained through the Human Trisome Project (University of Colorado Anschutz Medical Campus, COMIRB #15-2170, www.trisome.org). Plasma was collected in Vacutainer tubes (EDTA – purple capped or Lithium heparin – light green capped) and stored at -80°C. Participant medical history was collected by the respective biobanks.

Sample preparation

For plasma analyses (human and mouse plasma), a volume of 50 µl of was extracted in 450 µl of ice cold lysis buffer (methanol:acetonitrile:water 5:3:2). For cell experiments, $1x10^6$ cells were extracted in 1 ml of lysis buffer. In both protocols, incubation with lysis buffer was followed by vortexing for 30 minutes at 4ºC. Separate extraction for hydrophobic metabolites (including oxylipids) were performed in ice cold methanol with similar ratios and workflows. Insoluble proteins were pelleted by centrifugation (10 minutes at 4ºC and 10,000 x g) and supernatants were collected and stored at -80°C until analysis. UHPLC-MS metabolomics analyses were performed using a Vanquish UHPLC system coupled online to a Q Exactive mass spectrometer (Thermo Fisher, Bremen, Germany). Samples were resolved over a Kinetex C18 column (2.1 x 150 mm, 1.7 µm; Phenomenex, Torrance, CA, USA) at 25ºC using a three minute isocratic condition of 5% acetonitrile, 95% water, and 0.1% formic acid flowing at 250 µl/min,48 or using a 5 min gradient at 400 µl/min from 5-95% B (A: water/0.1% formic acid; B: acetonitrile/0.1% formic acid) and a 17 min gradient ((A) water/acetonitrile (75/25, vol/vol) with 5 mmol/L ammonium acetate and (B) 2-propanol/acetonitrile/water (50/45/5, vol/vol/vol) with 5 mmol/L ammonium acetate). Compounds of interest were monitored and quantified in negative ion mode against deuterium-labeled internal standards. MS analysis and data elaboration were performed as described (139, 140). To monitor possible technical variability, technical replicates were run for both cohorts. Briefly, for the plasma samples from each cohort, aliquots of each of the individual samples were combined to make technical replicates, which were run as described above. Additionally, in each experiment, several buffer aliquots were run as blanks for artifact identification.

Metabolomics data processing

Metabolite assignments and isotopologue distributions in tracing experiments with $^{13}C^{15}N$-tryptophan were performed using MAVEN (Princeton, NJ, USA) and Compound Discoverer (Thermo Fisher, Bremen, Germany), on the basis of accurate intact mass, retention time and MS/MS (141, 142). Peak areas were exported for further statistical analysis with R (R Foundation for Statistical Computing, Vienna, Austria). Data sets from each of the two studies were log2-transformed. To perform differential expression analysis, the limma R package was used

to fit a linear model to the data, including age, sex, and cohort as covariates (21). Log fold change, p-value and adjusted p-value were calculated for the T21-D21 comparison using the empirical Bayes function and Benjamini-Hochberg adjustment procedure for multiple testing correction in limma (143). Adjusted p-values shown in the volcano plots and reported on the box plots were generated with this limma moderated t-test. For displaying data per sample on the boxplots, we plotted the residuals from the model fit.

For pathway enrichment, we first mapped the 91 metabolites to KEGG pathways using the KEGGREST R package (144). Of the 91 metabolites, 79 were annotated to at least one KEGG pathway. In total, this resulted in 116 unique pathway annotations which had at least 1 metabolite in them from the set of 79. We excluded pathways with less than 5 metabolites in them, leaving 52 pathways to investigate. Using this set of pathways, we performed a hypergeometric test in which the 16 differentially abundant metabolites were selected from the 79. For each pathway, we tested the number of metabolites that were both in the pathway and differentially abundant.

Predictive modeling

To select metabolites to be used as features for predictive modeling, we used the age-, sex-, and cohort-adjusted metabolomics data. Missing values made up less than 1% of the data and were imputed with the k-nearest neighbors algorithm using k = 5. Imputation was performed within the karyotype group using the impute package in R (145). We trained 10,000 independent, 5-fold cross-validated lasso regression models on combined set of Nexus and HTP samples using the R, glmnet package (146). For each independently trained model, metabolite coefficients and model accuracy was recorded. For models which reached 90% accuracy or greater, we recorded which metabolites had non-zero coefficients (i.e. features selected in the model). To select our final set of biomarkers to test, we used metabolites which had been selected by at least 80% of the models reaching 90% accuracy or greater, resulting in 11 total metabolites. We then evaluated the performance of building a predictor using the lasso model with the top 11 identified metabolites. To estimate performance, we ran a bootstrapped analysis over 10,000 independently trained models. We randomly separated the 169 patient samples into 80% training and 20% testing sets. Using the 11 metabolites, we used 5-fold cross-validation on the training set to identify the optimal value, then tested the trained model on the held-out testing set. We reported the average model performance over the 10,000 models and provide an empirically determined (from the bootstrapped analysis) 95% confidence intervals. Area under the receiver operating characteristic curve (AUC) is reported.

Data and code availability

All data and R code developed for the full set of statistical and machine learning analyses is available at: https://github.com/CostelloLab/Trisomy21_KYN_metabolomics. To ensure reproducibility, this code can be run to generate all figures for this manuscript.

Cell culture

Human fibroblasts were described previously (11). For the metabolic flux experiment, cells were cultured in 5 mg/L $^{13}C_{11}$ $^{15}N_2$ L-tryptophan (Sigma-Aldrich Cat #574597) for 72 hr prior to stimulation with 10 ng/mL IFN-α (R&D Systems Cat# 11101-2). Media was prepared by adding 120 uL of 10 mg/mL stock $^{13}C_{11}$ $^{15}N_2$ L-

tryptophan in 1x PBS to 240 mL of RPMI (Corning Cat# 10-040) in 10% Dialyzed FBS (Sigma Cat# F0392) and 1x Anti-Anti (Gibco Cat# 15240-062). Cells were treated with 10 ng/mL IFN-α or vehicle by adding 6 uL of 0.2 mg/mL IFN-α or 1x PBS to 120 mL of heavy labeled media. Cell lysates and media were collected at 0, 1, 6, and 24 hours following initial application of the heavy tryptophan and IFN-α. LC-MS metabolomics profiling was performed as described above, and tryptophan catabolites were identified by their C13 and/or N15 peaks.

Western blots

Cells were plated at equal densities (~33,000/cm^2) and allowed to attach overnight. The next day, IFN-α (R&D Systems Cat# 11101-2) was added at 10 ng/mL in RPMI (Corning Cat# 10-040) and cells were harvested by 0.25% trypsin (Gibco Cat# 25200-056) at 0, 1, 6, and 24 hours. Trypsin was quenched by adding RPMI with 10% Dialyzed FBS (Sigma Cat# F0392). Cells were pelleted at 200g for 5 minutes. Cell pellets were washed with 1x PBS, then resuspended in RIPA buffer containing 1 µg/mL pepstatin, 2 µg/mL aprotonin, 20 µg/mL trypsin inhibitor, 10 nM leupeptin, 200 nM Na3VO4, 500 nM phenylmethylsulfonyl fluoride (PMSF), and 10 µM NaF. Suspensions were sonicated at six watts for 15 s two times and clarified by centrifugation at 21,000 g for 10 min at 4°C. Supernatants were quantified in a Pierce BCA Protein Assay and diluted in complete RIPA with 4x Laemmli sample buffer. Tris-glycine SDS-polyacrylamide gel electrophoresis was used to separate 20–40 µg protein lysate, which was transferred to a 0.45 µm polyvinylidene fluoride (PVDF) membrane. Membranes were blocked in 5% non-fat dried milk or 2.5% bovine serum albumin (BSA) in Tris-buffered saline containing 0.1% TWEEN (TBS-T) at room temperature for 30 min. Immunoblotting was done using primary antibodies against Stat1 (Santa Cruz Biotechnology Cat# 346), pStat1 (Cell Signaling Technology Cat# 7649), IDO1 (Cell Signaling Technology Cat# 86630), and GAPDH (Santa Cruz Biotechnology Cat# 365062) overnight in 5% non-fat dried milk or 2.5% BSA in TBS-T at 4°C while shaking. Membranes were washed 3x in TBS-T for 5–15 min before probing with a horseradish peroxidase (HRP) conjugated secondary antibody in 5% non-fat dried milk at room temperature for one hour. Membranes were again washed 3x in TBS-T for 5–15 min before applying enhanced chemiluminescence (ECL) solution. Chemiluminensence signal was captured using a GE (Pittsburgh, PA) ImageQuant LAS4000.

Mouse strains

Dp(10)1Yey/+, Dp(16)1(Yey)/+ and Dp(17)1(Yey)/+ have been previously described (51). Dp(16) mice were purchased from Jackson Laboratories or provided by Drs. Faycal Guedj and Diana Bianchi at the National Institutes of Health. Dp(10)Yey/+, and Dp(17)1(Yey)/+ mice were provided by Drs. Katheleen Gardiner and Santos Franco, respectively. Animals were used between 6 and 30 weeks of age. All mice were maintained on a C57Bl/6 background and housed in specific-pathogen-free conditions. All experiments were approved by the Institutional Animal Care and Use Committee at the University of Colorado Anschutz Medical Campus.

Poly(I:C) treatment

Mice were allocated into control and poly(I:C) groups according to age, sex, and genotype. VacciGrade^{TM} high molecular weight poly(I:C) (InvivoGen Cat# vac-pic) was diluted to 1 mg/mL, according to manufacturer's

instructions. For induction of chronic inflammation, mice received intraperitoneal injections of 10 µg/g poly(I:C) at two-day intervals for a total of nine injections. Blood was either collected prior to the final injection, via the submandibular vein into 0.5 mL of 18 u/mL sodium heparin (Sigma Cat# H3393) or after sacrifice via cardiac puncture into 1.3 mL lithium heparin tubes (Fisher Cat #41-12-17-02). Blood samples were centrifuged (700 x g, 15 mins, 21°C) to separate the plasma. Plasma was collected into a fresh tube and centrifuged (2200 x g, 15 mins, 21°C) to pellet any remaining cells; cell-free plasma was aliquoted and stored at -80°C.

Acknowledgements. This work was supported primarily by the Linda Crnic Institute for Down Syndrome, the Global Down Syndrome Foundation, the Anna and John J. Sie Foundation, the Boettcher Foundation, and the University of Colorado School of Medicine. We thank the individuals with Down syndrome that donated the biological samples that enabled these studies.

ADDITIONAL INFORMATION

Competing interests. JME: Reviewing Editor, eLife. The other authors declare no competing interests.

Funding. This work was supported primarily by the Linda Crnic Institute for Down Syndrome, the Global Down Syndrome Foundation, the Anna and John J. Sie Foundation, the Boettcher Foundation, and the University of Colorado School of Medicine. RKP is supported by NIH training grant T15LM009451.

Author Contributions. RKP**,** KDS, JME, and JCC, conception and design, acquisition of data, analysis and interpretation of data, drafting or revising the article; AD, conception and design, acquisition of data, analysis and interpretation of data; RCH, MPL, KPS, KAW, RM, KDT, ALR, REG, RBW, acquisition of data, analysis and interpretation of data.

REFERENCES.

1. Alexander M, Petri H, Ding Y, Wandel C, Khwaja O, Foskett N. Morbidity and medication in a large population of individuals with Down syndrome compared to the general population. Developmental medicine and child neurology. 2016;58(3):246-54. doi: 10.1111/dmcn.12868. PubMed PMID: 26282180.

2. de Sola S, de la Torre R, Sanchez-Benavides G, Benejam B, Cuenca-Royo A, Del Hoyo L, Rodriguez J, Catuara-Solarz S, Sanchez-Gutierrez J, Duenas-Espin I, Hernandez G, Pena-Casanova J, Langohr K, Videla S, Blehaut H, Farre M, Dierssen M, Group TS. A new cognitive evaluation battery for Down syndrome and its relevance for clinical trials. Frontiers in psychology. 2015;6:708. doi: 10.3389/fpsyg.2015.00708. PubMed PMID: 26089807; PMCID: 4455308.

3. Hartley D, Blumenthal T, Carrillo M, DiPaolo G, Esralew L, Gardiner K, Granholm AC, Iqbal K, Krams M, Lemere C, Lott I, Mobley W, Ness S, Nixon R, Potter H, Reeves R, Sabbagh M, Silverman W, Tycko B, Whitten M, Wisniewski T. Down syndrome and Alzheimer's disease: Common pathways, common goals. Alzheimers Dement. 2015;11(6):700-9. doi: 10.1016/j.jalz.2014.10.007. PubMed PMID: 25510383; PMCID: PMC4817997.

4. Kinik ST, Ozcay F, Varan B. Type I diabetes mellitus, Hashimoto's thyroiditis and celiac disease in an adolescent with Down syndrome. Pediatr Int. 2006;48(4):433-5. doi: 10.1111/j.1442-200X.2006.02238.x. PubMed PMID: 16911096.

5. Roizen NJ, Magyar CI, Kuschner ES, Sulkes SB, Druschel C, van Wijngaarden E, Rodgers L, Diehl A, Lowry R, Hyman SL. A community cross-sectional survey of medical problems in 440 children with Down syndrome in New York State. J Pediatr. 2014;164(4):871-5. doi: 10.1016/j.jpeds.2013.11.032. PubMed PMID: 24367984.

6. Sobey CG, Judkins CP, Sundararajan V, Phan TG, Drummond GR, Srikanth VK. Risk of Major Cardiovascular Events in People with Down Syndrome. PLoS One. 2015;10(9):e0137093. doi: 10.1371/journal.pone.0137093. PubMed PMID: 26421620; PMCID: 4589343.

7. Yang Q, Rasmussen SA, Friedman JM. Mortality associated with Down's syndrome in the USA from 1983 to 1997: a population-based study. Lancet. 2002;359(9311):1019-25. PubMed PMID: 11937181.

8. Hasle H, Clemmensen IH, Mikkelsen M. Risks of leukaemia and solid tumours in individuals with Down's syndrome. Lancet. 2000;355(9199):165-9. doi: 10.1016/S0140-6736(99)05264-2. PubMed PMID: 10675114.

9. Hasle H, Friedman JM, Olsen JH, Rasmussen SA. Low risk of solid tumors in persons with Down syndrome. Genetics in medicine : official journal of the American College of Medical Genetics. 2016;18(11):1151-7. Epub 2016/11/01. doi: 10.1038/gim.2016.23. PubMed PMID: 27031084.

10. Sinai A, Mokrysz C, Bernal J, Bohnen I, Bonell S, Courtenay K, Dodd K, Gazizova D, Hassiotis A, Hillier R, McBrien J, McCarthy J, Mukherji K, Naeem A, Perez-Achiaga N, Rantell K, Sharma V, Thomas D, Walker Z, Whitham S, Strydom A. Predictors of Age of Diagnosis and Survival of Alzheimer's Disease in Down Syndrome. J Alzheimers Dis. 2018;61(2):717-28. Epub 2017/12/12. doi: 10.3233/JAD-170624; PMCID: 29226868.

11. Sullivan KD, Lewis HC, Hill AA, Pandey A, Jackson LP, Cabral JM, Smith KP, Liggett LA, Gomez EB, Galbraith MD, DeGregori J, Espinosa JM. Trisomy 21 consistently activates the interferon response. Elife. 2016;5. doi: 10.7554/eLife.16220. PubMed PMID: 27472900.

12. Sullivan KD, Evans D, Pandey A, Hraha TH, Smith KP, Markham N, Rachubinski AL, Wolter-Warmerdam K, Hickey F, Espinosa JM, Blumenthal T. Trisomy 21 causes changes in the circulating proteome indicative of chronic autoinflammation. Scientific reports. 2017;7(1):14818. Epub 2017/11/03. doi: 10.1038/s41598-017-13858-3. PubMed PMID: 29093484; PMCID: PMC5665944.

13. Epstein LB, Epstein CJ. Localization fo the gene AVG for the antiviral expression of immune and classical interferon to the distal portion of the long arm of chromosome 21. The Journal of infectious diseases. 1976;133 Suppl:A56-62. Epub 1976/06/01. PubMed PMID: 180211.

14. Mills E, O'Neill LA. Succinate: a metabolic signal in inflammation. Trends in cell biology. 2014;24(5):313-20. Epub 2013/12/24. doi: 10.1016/j.tcb.2013.11.008. PubMed PMID: 24361092.

15. Ma S, Sun R, Jiang B, Gao J, Deng W, Liu P, He R, Cui J, Ji M, Yi W, Yang P, Wu X, Xiong Y, Qiu Z, Ye D, Guan KL. L2hgdh Deficiency Accumulates l-2-Hydroxyglutarate with Progressive Leukoencephalopathy and Neurodegeneration. Mol Cell Biol. 2017;37(8). Epub 2017/02/01. doi: 10.1128/MCB.00492-16. PubMed PMID: 28137912; PMCID: PMC5376639.

16. Guillemin GJ. Quinolinic acid, the inescapable neurotoxin. The FEBS journal. 2012;279(8):1356-65. Epub 2012/01/18. doi: 10.1111/j.1742-4658.2012.08485.x. PubMed PMID: 22248144.

17. Badawy AA. Kynurenine Pathway of Tryptophan Metabolism: Regulatory and Functional Aspects. Int J Tryptophan Res. 2017;10:1178646917691938. Epub 2017/05/05. doi: 10.1177/1178646917691938. PubMed PMID: 28469468; PMCID: PMC5398323.

18. Vecsei L, Szalardy L, Fulop F, Toldi J. Kynurenines in the CNS: recent advances and new questions. Nature reviews Drug discovery. 2013;12(1):64-82. Epub 2012/12/15. doi: 10.1038/nrd3793. PubMed PMID: 23237916.

19. Braidy N, Grant R. Kynurenine pathway metabolism and neuroinflammatory disease. Neural Regen Res. 2017;12(1):39-42. Epub 2017/03/03. doi: 10.4103/1673-5374.198971. PubMed PMID: 28250737; PMCID: PMC5319230.

20. Schwarcz R, Stone TW. The kynurenine pathway and the brain: Challenges, controversies and promises. Neuropharmacology. 2017;112(Pt B):237-47. Epub 2016/08/12. doi: 10.1016/j.neuropharm.2016.08.003. PubMed PMID: 27511838.

21. Ritchie ME, Phipson B, Wu D, Hu Y, Law CW, Shi W, Smyth GK. limma powers differential expression analyses for RNA-sequencing and microarray studies. Nucleic Acids Res. 2015;43(7):e47. Epub 2015/01/22. doi: 10.1093/nar/gkv007. PubMed PMID: 25605792; PMCID: PMC4402510.

22. Lejeune J, Rethore MO, de Blois MC, Peeters M, Naffah J, Megarbane A, Cattaneo F, Mircher C, Rabier D, Parvy P, et al. [Amino acids and trisomy 21]. Annales de genetique. 1992;35(1):8-13. Epub 1992/01/01. PubMed PMID: 1535189.

23. Caracausi M, Ghini V, Locatelli C, Mericio M, Piovesan A, Antonaros F, Pelleri MC, Vitale L, Vacca RA, Bedetti F, Mimmi MC, Luchinat C, Turano P, Strippoli P, Cocchi G. Plasma and urinary metabolomic profiles of Down syndrome correlate with alteration of mitochondrial metabolism. Scientific reports. 2018;8(1):2977. Epub 2018/02/16. doi: 10.1038/s41598-018-20834-y. PubMed PMID: 29445163; PMCID: PMC5813015.

24. Chadefaux B, Ceballos I, Hamet M, Coude M, Poissonnier M, Kamoun P, Allard D. Is absence of atheroma in Down syndrome due to decreased homocysteine levels? Lancet. 1988;2(8613):741. Epub 1988/09/24. PubMed PMID: 2901588.

25. Wilson JX. The physiological role of dehydroascorbic acid. FEBS letters. 2002;527(1-3):5-9. Epub 2002/09/11. PubMed PMID: 12220624.

26. Andre P, Villain F. Free radical scavenging properties of mannitol and its role as a constituent of hyaluronic acid fillers: a literature review. Int J Cosmet Sci. 2017;39(4):355-60. Epub 2016/12/28. doi: 10.1111/ics.12386. PubMed PMID: 28027572.

27. Kanehisa M, Furumichi M, Tanabe M, Sato Y, Morishima K. KEGG: new perspectives on genomes, pathways, diseases and drugs. Nucleic Acids Res. 2017;45(D1):D353-D61. Epub 2016/12/03. doi: 10.1093/nar/gkw1092. PubMed PMID: 27899662; PMCID: PMC5210567.

28. Tibshirani R. The lasso method for variable selection in the Cox model. Statistics in medicine. 1997;16(4):385-95. Epub 1997/02/28. PubMed PMID: 9044528.

29. Davis I, Liu A. What is the tryptophan kynurenine pathway and why is it important to neurotherapeutics? Expert Rev Neurother. 2015;15(7):719-21. Epub 2015/05/26. doi: 10.1586/14737175.2015.1049999. PubMed PMID: 26004930; PMCID: PMC4482796.

30. O'Mahony SM, Clarke G, Borre YE, Dinan TG, Cryan JF. Serotonin, tryptophan metabolism and the brain-gut-microbiome axis. Behav Brain Res. 2015;277:32-48. Epub 2014/08/01. doi: 10.1016/j.bbr.2014.07.027. PubMed PMID: 25078296.

31. Li G, Young KD. Indole production by the tryptophanase TnaA in Escherichia coli is determined by the amount of exogenous tryptophan. Microbiology. 2013;159(Pt 2):402-10. Epub 2013/02/12. doi: 10.1099/mic.0.064139-0. PubMed PMID: 23397453.

32. Guillemin GJ, Brew BJ. Implications of the kynurenine pathway and quinolinic acid in Alzheimer's disease. Redox Rep. 2002;7(4):199-206. Epub 2002/10/25. doi: 10.1179/135100002125000550. PubMed PMID: 12396664.

33. Guillemin GJ, Williams KR, Smith DG, Smythe GA, Croitoru-Lamoury J, Brew BJ. Quinolinic acid in the pathogenesis of Alzheimer's disease. Advances in experimental medicine and biology. 2003;527:167-76. Epub 2004/06/23. PubMed PMID: 15206729.

34. Rahman A, Ting K, Cullen KM, Braidy N, Brew BJ, Guillemin GJ. The excitotoxin quinolinic acid induces tau phosphorylation in human neurons. PLoS One. 2009;4(7):e6344. Epub 2009/07/23. doi: 10.1371/journal.pone.0006344. PubMed PMID: 19623258; PMCID: PMC2709912.

35. Gulaj E, Pawlak K, Bien B, Pawlak D. Kynurenine and its metabolites in Alzheimer's disease patients. Adv Med Sci. 2010;55(2):204-11. Epub 2010/07/20. doi: 10.2478/v10039-010-0023-6. PubMed PMID: 20639188.

36. Beal MF, Matson WR, Swartz KJ, Gamache PH, Bird ED. Kynurenine pathway measurements in Huntington's disease striatum: evidence for reduced formation of kynurenic acid. Journal of neurochemistry. 1990;55(4):1327-39. Epub 1990/10/01. PubMed PMID: 2144582.

37. Stoy N, Mackay GM, Forrest CM, Christofides J, Egerton M, Stone TW, Darlington LG. Tryptophan metabolism and oxidative stress in patients with Huntington's disease. Journal of neurochemistry. 2005;93(3):611-23. Epub 2005/04/20. doi: 10.1111/j.1471-4159.2005.03070.x. PubMed PMID: 15836620.

38. Guillemin GJ, Kerr SJ, Brew BJ. Involvement of quinolinic acid in AIDS dementia complex. Neurotox Res. 2005;7(1-2):103-23. Epub 2005/01/11. PubMed PMID: 15639803.

39. Davies NW, Guillemin G, Brew BJ. Tryptophan, Neurodegeneration and HIV-Associated Neurocognitive Disorder. Int J Tryptophan Res. 2010;3:121-40. Epub 2010/01/01. PubMed PMID: 22084594; PMCID: PMC3195234.

40. Kandanearatchi A, Brew BJ. The kynurenine pathway and quinolinic acid: pivotal roles in HIV associated neurocognitive disorders. The FEBS journal. 2012;279(8):1366-74. Epub 2012/01/21. doi: 10.1111/j.1742-4658.2012.08500.x. PubMed PMID: 22260426.

41. Zinger A, Barcia C, Herrero MT, Guillemin GJ. The involvement of neuroinflammation and kynurenine pathway in Parkinson's disease. Parkinsons Dis. 2011;2011:716859. Epub 2011/06/21. doi: 10.4061/2011/716859. PubMed PMID: 21687761; PMCID: PMC3109408.

42. Guillemin GJ, Meininger V, Brew BJ. Implications for the kynurenine pathway and quinolinic acid in amyotrophic lateral sclerosis. Neurodegener Dis. 2005;2(3-4):166-76. Epub 2006/08/16. doi: 10.1159/000089622. PubMed PMID: 16909022.

43. Chen Y, Stankovic R, Cullen KM, Meininger V, Garner B, Coggan S, Grant R, Brew BJ, Guillemin GJ. The kynurenine pathway and inflammation in amyotrophic lateral sclerosis. Neurotox Res. 2010;18(2):132-42. Epub 2009/11/19. doi: 10.1007/s12640-009-9129-7. PubMed PMID: 19921535.

44. Hartai Z, Klivenyi P, Janaky T, Penke B, Dux L, Vecsei L. Kynurenine metabolism in multiple sclerosis. Acta Neurol Scand. 2005;112(2):93-6. Epub 2005/07/13. doi: 10.1111/j.1600-0404.2005.00442.x. PubMed PMID: 16008534.

45. Lim CK, Brew BJ, Sundaram G, Guillemin GJ. Understanding the roles of the kynurenine pathway in multiple sclerosis progression. Int J Tryptophan Res. 2010;3:157-67. Epub 2010/01/01. PubMed PMID: 22084596; PMCID: PMC3195238.

46. Guillemin GJ, Kerr SJ, Pemberton LA, Smith DG, Smythe GA, Armati PJ, Brew BJ. IFN-beta1b induces kynurenine pathway metabolism in human macrophages: potential implications for multiple sclerosis treatment. Journal of interferon & cytokine research : the official journal of the International Society for Interferon and Cytokine Research. 2001;21(12):1097-101. Epub 2002/01/19. doi: 10.1089/107999001317205231. PubMed PMID: 11798468.

47. Connor TJ, Starr N, O'Sullivan JB, Harkin A. Induction of indolamine 2,3-dioxygenase and kynurenine 3-monooxygenase in rat brain following a systemic inflammatory challenge: a role for IFN-gamma? Neuroscience letters. 2008;441(1):29-34. Epub 2008/07/01. doi: 10.1016/j.neulet.2008.06.007. PubMed PMID: 18584961.

48. Taylor MW, Feng GS. Relationship between interferon-gamma, indoleamine 2,3-dioxygenase, and tryptophan catabolism. FASEB journal : official publication of the Federation of American Societies for Experimental Biology. 1991;5(11):2516-22. Epub 1991/08/01. PubMed PMID: 1907934.

49. Hassanain HH, Chon SY, Gupta SL. Differential regulation of human indoleamine 2,3-dioxygenase gene expression by interferons-gamma and -alpha. Analysis of the regulatory region of the gene and identification of an interferon-gamma-inducible DNA-binding factor. J Biol Chem. 1993;268(7):5077-84. Epub 1993/03/05. PubMed PMID: 8444884.

50. Wichers MC, Maes M. The role of indoleamine 2,3-dioxygenase (IDO) in the pathophysiology of interferon-alpha-induced depression. Journal of psychiatry & neuroscience : JPN. 2004;29(1):11-7. PubMed PMID: 14719046; PMCID: 305266.

51. Yu T, Liu C, Belichenko P, Clapcote SJ, Li S, Pao A, Kleschevnikov A, Bechard AR, Asrar S, Chen R, Fan N, Zhou Z, Jia Z, Chen C, Roder JC, Liu B, Baldini A, Mobley WC, Yu YE. Effects of individual segmental trisomies of human chromosome 21 syntenic regions on hippocampal long-term potentiation and cognitive behaviors in mice. Brain research. 2010;1366:162-71. doi: 10.1016/j.brainres.2010.09.107. PubMed PMID: 20932954; PMCID: 3027718.

52. Aziz NM, Guedj F, Pennings JLA, Olmos-Serrano JL, Siegel A, Haydar TF, Bianchi DW. Lifespan analysis of brain development, gene expression and behavioral phenotypes in the Ts1Cje, Ts65Dn and Dp(16)1/Yey

mouse models of Down syndrome. Dis Model Mech. 2018;11(6). Epub 2018/05/03. doi: 10.1242/dmm.031013. PubMed PMID: 29716957; PMCID: PMC6031353.

53. Pietras EM, Lakshminarasimhan R, Techner JM, Fong S, Flach J, Binnewies M, Passegue E. Re-entry into quiescence protects hematopoietic stem cells from the killing effect of chronic exposure to type I interferons. The Journal of experimental medicine. 2014;211(2):245-62. Epub 2014/02/05. doi: 10.1084/jem.20131043. PubMed PMID: 24493802; PMCID: PMC3920566.

54. Pichlmair A, Reis e Sousa C. Innate recognition of viruses. Immunity. 2007;27(3):370-83. Epub 2007/09/26. doi: 10.1016/j.immuni.2007.08.012. PubMed PMID: 17892846.

55. Zimmermann M, Arruda-Silva F, Bianchetto-Aguilera F, Finotti G, Calzetti F, Scapini P, Lunardi C, Cassatella MA, Tamassia N. IFNalpha enhances the production of IL-6 by human neutrophils activated via TLR8. Scientific reports. 2016;6:19674. doi: 10.1038/srep19674. PubMed PMID: 26790609; PMCID: 4726390.

56. Vila-del Sol V, Punzon C, Fresno M. IFN-gamma-induced TNF-alpha expression is regulated by interferon regulatory factors 1 and 8 in mouse macrophages. Journal of immunology. 2008;181(7):4461-70. Epub 2008/09/20. PubMed PMID: 18802049.

57. Luster AD, Ravetch JV. Genomic Characterization of a Gamma-Interferon-Inducible Gene (Ip-10) and Identification of an Interferon-Inducible Hypersensitive Site. Mol Cell Biol. 1987;7(10):3723-31. doi: Doi 10.1128/Mcb.7.10.3723. PubMed PMID: WOS:A1987K217400043.

58. Bosco MC, Gusella GL, Espinoza-Delgado I, Longo DL, Varesio L. Interferon-gamma upregulates interleukin-8 gene expression in human monocytic cells by a posttranscriptional mechanism. Blood. 1994;83(2):537-42. Epub 1994/01/15. PubMed PMID: 8286750.

59. Li C, Goodrich JM, Yang X. Interferon-gamma (IFN-gamma) regulates production of IL-10 and IL-12 in human herpesvirus-6 (HHV-6)-infected monocyte/macrophage lineage. Clin Exp Immunol. 1997;109(3):421-5. Epub 1997/10/27. PubMed PMID: 9328116; PMCID: PMC1904766.

60. Bug G, Aman MJ, Tretter T, Huber C, Peschel C. Induction of macrophage-inflammatory protein 1alpha (MIP-1alpha) by interferon-alpha. Exp Hematol. 1998;26(2):117-23. Epub 1998/02/24. PubMed PMID: 9472801.

61. Zhou ZH, Han Y, Wei T, Aras S, Chaturvedi P, Tyler S, Rani MR, Ransohoff RM. Regulation of monocyte chemoattractant protein (MCP)-1 transcription by interferon-gamma (IFN-gamma) in human astrocytoma cells: postinduction refractory state of the gene, governed by its upstream elements. FASEB journal : official publication

of the Federation of American Societies for Experimental Biology. 2001;15(2):383-92. Epub 2001/02/07. doi: 10.1096/fj.00-0373com. PubMed PMID: 11156954.

62. Horikawa T, Nakayama T, Hikita I, Yamada H, Fujisawa R, Bito T, Harada S, Fukunaga A, Chantry D, Gray PW, Morita A, Suzuki R, Tezuka T, Ichihashi M, Yoshie O. IFN-gamma-inducible expression of thymus and activation-regulated chemokine/CCL17 and macrophage-derived chemokine/CCL22 in epidermal keratinocytes and their roles in atopic dermatitis. International immunology. 2002;14(7):767-73. Epub 2002/07/04. PubMed PMID: 12096036.

63. Wiesemann E, Sonmez D, Heidenreich F, Windhagen A. Interferon-beta increases the stimulatory capacity of monocyte-derived dendritic cells to induce IL-13, IL-5 and IL-10 in autologous T-cells. Journal of neuroimmunology. 2002;123(1-2):160-9. Epub 2002/03/07. PubMed PMID: 11880160.

64. Strengell M, Julkunen I, Matikainen S. IFN-alpha regulates IL-21 and IL-21R expression in human NK and T cells. J Leukoc Biol. 2004;76(2):416-22. Epub 2004/06/05. doi: 10.1189/jlb.1003488. PubMed PMID: 15178704.

65. Iwamoto T, Okamoto H, Kobayashi S, Ikari K, Toyama Y, Tomatsu T, Kamatani N, Momohara S. A role of monocyte chemoattractant protein-4 (MCP-4)/CCL13 from chondrocytes in rheumatoid arthritis. The FEBS journal. 2007;274(18):4904-12. Epub 2007/09/11. doi: 10.1111/j.1742-4658.2007.06013.x. PubMed PMID: 17824960.

66. Feld M, Shpacovitch VM, Fastrich M, Cevikbas F, Steinhoff M. Interferon-gamma induces upregulation and activation of the interleukin-31 receptor in human dermal microvascular endothelial cells. Experimental dermatology. 2010;19(10):921-3. Epub 2010/09/21. doi: 10.1111/j.1600-0625.2010.01147.x. PubMed PMID: 20849534.

67. Joubert P, Lajoie-Kadoch S, Wellemans V, Letuve S, Tulic MK, Halayko AJ, Hamid Q. Expression and regulation of CCL15 by human airway smooth muscle cells. Clin Exp Allergy. 2012;42(1):85-94. Epub 2011/11/19. doi: 10.1111/j.1365-2222.2011.03894.x. PubMed PMID: 22092970.

68. Blahoianu MA, Rahimi AA, Kozlowski M, Angel JB, Kumar A. IFN-gamma-induced IL-27 and IL-27p28 expression are differentially regulated through JNK MAPK and PI3K pathways independent of Jak/STAT in human monocytic cells. Immunobiology. 2014;219(1):1-8. Epub 2013/07/31. doi: 10.1016/j.imbio.2013.06.001. PubMed PMID: 23891538.

69. Kopach P, Lockatell V, Pickering EM, Haskell RE, Anderson RD, Hasday JD, Todd NW, Luzina IG, Atamas SP. IFN-gamma directly controls IL-33 protein level through a STAT1- and LMP2-dependent mechanism. J Biol Chem. 2014;289(17):11829-43. Epub 2014/03/13. doi: 10.1074/jbc.M113.534396. PubMed PMID: 24619410; PMCID: PMC4002090.

70. Wiseman FK, Al-Janabi T, Hardy J, Karmiloff-Smith A, Nizetic D, Tybulewicz VL, Fisher EM, Strydom A. A genetic cause of Alzheimer disease: mechanistic insights from Down syndrome. Nat Rev Neurosci. 2015;16(9):564-74. doi: 10.1038/nrn3983. PubMed PMID: 26243569.

71. Head E, Lott IT, Wilcock DM, Lemere CA. Aging in Down Syndrome and the Development of Alzheimer's Disease Neuropathology. Curr Alzheimer Res. 2016;13(1):18-29. PubMed PMID: 26651341; PMCID: PMC4948181.

72. Johannsen P, Christensen JE, Goldstein H, Nielsen VK, Mai J. Epilepsy in Down syndrome--prevalence in three age groups. Seizure. 1996;5(2):121-5. PubMed PMID: 8795127.

73. Walker JC, Dosen A, Buitelaar JK, Janzing JG. Depression in Down syndrome: a review of the literature. Research in developmental disabilities. 2011;32(5):1432-40. doi: 10.1016/j.ridd.2011.02.010. PubMed PMID: 21392935.

74. DiGuiseppi C, Hepburn S, Davis JM, Fidler DJ, Hartway S, Lee NR, Miller L, Ruttenber M, Robinson C. Screening for autism spectrum disorders in children with Down syndrome: population prevalence and screening test characteristics. J Dev Behav Pediatr. 2010;31(3):181-91. doi: 10.1097/DBP.0b013e3181d5aa6d. PubMed PMID: 20375732; PMCID: PMC4419691.

75. Ji NY, Capone GT, Kaufmann WE. Autism spectrum disorder in Down syndrome: cluster analysis of Aberrant Behaviour Checklist data supports diagnosis. J Intellect Disabil Res. 2011;55(11):1064-77. doi: 10.1111/j.1365-2788.2011.01465.x. PubMed PMID: 21883598.

76. Bagyinszky E, Youn YC, An SS, Kim S. The genetics of Alzheimer's disease. Clinical interventions in aging. 2014;9:535-51. doi: 10.2147/CIA.S51571. PubMed PMID: 24729694; PMCID: 3979693.

77. Sleegers K, Brouwers N, Gijselinck I, Theuns J, Goossens D, Wauters J, Del-Favero J, Cruts M, van Duijn CM, Van Broeckhoven C. APP duplication is sufficient to cause early onset Alzheimer's dementia with cerebral amyloid angiopathy. Brain. 2006;129(Pt 11):2977-83. doi: 10.1093/brain/awl203. PubMed PMID: 16921174.

78. Johannsen P, Christensen JE, Mai J. The prevalence of dementia in Down syndrome. Dementia. 1996;7(4):221-5. PubMed PMID: 8835887.

79. Schupf N, Sergievsky GH. Genetic and host factors for dementia in Down's syndrome. The British journal of psychiatry : the journal of mental science. 2002;180:405-10. PubMed PMID: 11983636.

80. Zhang Y, Che M, Yuan J, Yu Y, Cao C, Qin XY, Cheng Y. Aberrations in circulating inflammatory cytokine levels in patients with Down syndrome: a meta-analysis. Oncotarget. 2017;8(48):84489-96. Epub 2017/11/16. doi: 10.18632/oncotarget.21060. PubMed PMID: 29137441; PMCID: PMC5663613.

81. Delneste Y, Charbonnier P, Herbault N, Magistrelli G, Caron G, Bonnefoy JY, Jeannin P. Interferon-gamma switches monocyte differentiation from dendritic cells to macrophages. Blood. 2003;101(1):143-50. doi: 10.1182/blood-2002-04-1164. PubMed PMID: 12393446.

82. Jordan WJ, Eskdale J, Boniotto M, Rodia M, Kellner D, Gallagher G. Modulation of the human cytokine response by interferon lambda-1 (IFN-lambda1/IL-29). Genes and immunity. 2007;8(1):13-20. doi: 10.1038/sj.gene.6364348. PubMed PMID: 17082759.

83. Fridman JS, Scherle PA, Collins R, Burn TC, Li Y, Li J, Covington MB, Thomas B, Collier P, Favata MF, Wen X, Shi J, McGee R, Haley PJ, Shepard S, Rodgers JD, Yeleswaram S, Hollis G, Newton RC, Metcalf B, Friedman SM, Vaddi K. Selective inhibition of JAK1 and JAK2 is efficacious in rodent models of arthritis: preclinical characterization of INCB028050. Journal of immunology. 2010;184(9):5298-307. doi: 10.4049/jimmunol.0902819. PubMed PMID: 20363976.

84. Schwarz MJ, Guillemin GJ, Teipel SJ, Buerger K, Hampel H. Increased 3-hydroxykynurenine serum concentrations differentiate Alzheimer's disease patients from controls. Eur Arch Psychiatry Clin Neurosci. 2013;263(4):345-52. Epub 2012/11/30. doi: 10.1007/s00406-012-0384-x. PubMed PMID: 23192697.

85. Majlath Z, Toldi J, Vecsei L. The potential role of kynurenines in Alzheimer's disease: pathomechanism and therapeutic possibilities by influencing the glutamate receptors. Journal of neural transmission. 2014;121(8):881-9. Epub 2013/12/19. doi: 10.1007/s00702-013-1135-5. PubMed PMID: 24346138.

86. Cupples CG, Tan YH. Effect of human interferon preparations on lymphoblastogenesis in Down's syndrome. Nature. 1977;267(5607):165-7. doi: 10.1038/267165a0. PubMed PMID: 16073432.

87. Maroun LE. Interferon-mediated effect on ribosomal RNA metabolism. Biochim Biophys Acta. 1978;517(1):109-14. PubMed PMID: 623751.

88. Maroun LE. Interferon effect on ribosomal ribonucleic acid related to chromosome 21 ploidy. Biochem J. 1979;179(1):221-5. PubMed PMID: 475756; PMCID: 1186612.

89. Maroun LE. Anti-interferon immunoglobulins can improve the trisomy 16 mouse phenotype. Teratology. 1995;51(5):329-35. doi: 10.1002/tera.1420510509. PubMed PMID: 7482354.

90. Hallam DM, Maroun LE. Anti-gamma interferon can prevent the premature death of trisomy 16 mouse cortical neurons in culture. Neuroscience letters. 1998;252(1):17-20. PubMed PMID: 9756348.

91. Maroun LE, Heffernan TN, Hallam DM. Partial IFN-alpha/beta and IFN-gamma receptor knockout trisomy 16 mouse fetuses show improved growth and cultured neuron viability. Journal of interferon & cytokine research : the official journal of the International Society for Interferon and Cytokine Research. 2000;20(2):197-203. doi: 10.1089/107999000312612. PubMed PMID: 10714556.

92. Epstein CJ, Weil J, Epstein LB. Abnormalities in the interferon response and immune systems in Down syndrome: studies in human trisomy 21 and mouse trisomy 16. Prog Clin Biol Res. 1987;246:191-208. Epub 1987/01/01. PubMed PMID: 2443929.

93. Epstein CJ. 2001 William Allan Award Address. From Down syndrome to the "human" in "human genetics". Am J Hum Genet. 2002;70(2):300-13. Epub 2002/01/16. PubMed PMID: 11791206; PMCID: PMC384910.

94. Tan YH, Schneider EL, Tischfield J, Epstein CJ, Ruddle FH. Human chromosome 21 dosage: effect on the expression of the interferon induced antiviral state. Science. 1974;186(4158):61-3. Epub 1974/10/04. PubMed PMID: 4371269.

95. Hong HS, Hwang EM, Sim HJ, Cho HJ, Boo JH, Oh SS, Kim SU, Mook-Jung I. Interferon gamma stimulates beta-secretase expression and sAPPbeta production in astrocytes. Biochem Biophys Res Commun. 2003;307(4):922-7. PubMed PMID: 12878199.

96. Minter MR, Moore Z, Zhang M, Brody KM, Jones NC, Shultz SR, Taylor JM, Crack PJ. Deletion of the type-1 interferon receptor in APPSWE/PS1DeltaE9 mice preserves cognitive function and alters glial phenotype. Acta neuropathologica communications. 2016;4(1):72. doi: 10.1186/s40478-016-0341-4. PubMed PMID: 27400725; PMCID: 4940712.

97. Browne TC, McQuillan K, McManus RM, O'Reilly JA, Mills KH, Lynch MA. IFN-gamma Production by amyloid beta-specific Th1 cells promotes microglial activation and increases plaque burden in a mouse model

of Alzheimer's disease. Journal of immunology. 2013;190(5):2241-51. doi: 10.4049/jimmunol.1200947. PubMed PMID: 23365075.

98. Yamamoto M, Kiyota T, Horiba M, Buescher JL, Walsh SM, Gendelman HE, Ikezu T. Interferon-gamma and tumor necrosis factor-alpha regulate amyloid-beta plaque deposition and beta-secretase expression in Swedish mutant APP transgenic mice. The American journal of pathology. 2007;170(2):680-92. doi: 10.2353/ajpath.2007.060378. PubMed PMID: 17255335; PMCID: 1851864.

99. Taylor JM, Minter MR, Newman AG, Zhang M, Adlard PA, Crack PJ. Type-1 interferon signaling mediates neuro-inflammatory events in models of Alzheimer's disease. Neurobiology of aging. 2014;35(5):1012-23. doi: 10.1016/j.neurobiolaging.2013.10.089. PubMed PMID: 24262201.

100. Breda C, Sathyasaikumar KV, Sograte Idrissi S, Notarangelo FM, Estranero JG, Moore GG, Green EW, Kyriacou CP, Schwarcz R, Giorgini F. Tryptophan-2,3-dioxygenase (TDO) inhibition ameliorates neurodegeneration by modulation of kynurenine pathway metabolites. Proc Natl Acad Sci U S A. 2016;113(19):5435-40. Epub 2016/04/27. doi: 10.1073/pnas.1604453113. PubMed PMID: 27114543; PMCID: PMC4868470.

101. Ellis B, Hye A, Snowden SG. Metabolic Modifications in Human Biofluids Suggest the Involvement of Sphingolipid, Antioxidant, and Glutamate Metabolism in Alzheimer's Disease Pathogenesis. J Alzheimers Dis. 2015;46(2):313-27. Epub 2015/04/04. doi: 10.3233/JAD-141899. PubMed PMID: 25835424.

102. Kaddurah-Daouk R, Rozen S, Matson W, Han X, Hulette CM, Burke JR, Doraiswamy PM, Welsh-Bohmer KA. Metabolomic changes in autopsy-confirmed Alzheimer's disease. Alzheimers Dement. 2011;7(3):309-17. Epub 2010/11/16. doi: 10.1016/j.jalz.2010.06.001. PubMed PMID: 21075060; PMCID: PMC3061205.

103. Kaddurah-Daouk R, Zhu H, Sharma S, Bogdanov M, Rozen SG, Matson W, Oki NO, Motsinger-Reif AA, Churchill E, Lei Z, Appleby D, Kling MA, Trojanowski JQ, Doraiswamy PM, Arnold SE, Pharmacometabolomics Research N. Alterations in metabolic pathways and networks in Alzheimer's disease. Transl Psychiatry. 2013;3:e244. Epub 2013/04/11. doi: 10.1038/tp.2013.18. PubMed PMID: 23571809; PMCID: PMC3641405.

104. Trushina E, Mielke MM. Recent advances in the application of metabolomics to Alzheimer's Disease. Biochim Biophys Acta. 2014;1842(8):1232-9. Epub 2013/07/03. doi: 10.1016/j.bbadis.2013.06.014. PubMed PMID: 23816564; PMCID: PMC3842412.

105. Zwilling D, Huang SY, Sathyasaikumar KV, Notarangelo FM, Guidetti P, Wu HQ, Lee J, Truong J, Andrews-Zwilling Y, Hsieh EW, Louie JY, Wu T, Scearce-Levie K, Patrick C, Adame A, Giorgini F, Moussaoui S, Laue G, Rassoulpour A, Flik G, Huang Y, Muchowski JM, Masliah E, Schwarcz R, Muchowski PJ. Kynurenine 3-monooxygenase inhibition in blood ameliorates neurodegeneration. Cell. 2011;145(6):863-74. Epub 2011/06/07. doi: 10.1016/j.cell.2011.05.020. PubMed PMID: 21640374; PMCID: PMC3118409.

106. Souza LC, Jesse CR, Antunes MS, Ruff JR, de Oliveira Espinosa D, Gomes NS, Donato F, Giacomeli R, Boeira SP. Indoleamine-2,3-dioxygenase mediates neurobehavioral alterations induced by an intracerebroventricular injection of amyloid-beta1-42 peptide in mice. Brain Behav Immun. 2016;56:363-77. doi: 10.1016/j.bbi.2016.03.002. PubMed PMID: 26965653.

107. Yu D, Tao BB, Yang YY, Du LS, Yang SS, He XJ, Zhu YW, Yan JK, Yang Q. The IDO inhibitor coptisine ameliorates cognitive impairment in a mouse model of Alzheimer's disease. J Alzheimers Dis. 2015;43(1):291-302. doi: 10.3233/JAD-140414. PubMed PMID: 25079795.

108. de Oliveira DL, Horn JF, Rodrigues JM, Frizzo ME, Moriguchi E, Souza DO, Wofchuk S. Quinolinic acid promotes seizures and decreases glutamate uptake in young rats: reversal by orally administered guanosine. Brain research. 2004;1018(1):48-54. Epub 2004/07/21. doi: 10.1016/j.brainres.2004.05.033. PubMed PMID: 15262204.

109. Schmidt AP, Lara DR, de Faria Maraschin J, da Silveira Perla A, Onofre Souza D. Guanosine and GMP prevent seizures induced by quinolinic acid in mice. Brain research. 2000;864(1):40-3. Epub 2000/05/04. PubMed PMID: 10793184.

110. Schwarcz R, Brush GS, Foster AC, French ED. Seizure activity and lesions after intrahippocampal quinolinic acid injection. Experimental neurology. 1984;84(1):1-17. Epub 1984/04/01. PubMed PMID: 6705878.

111. Lapin IP. Kynurenines and seizures. Epilepsia. 1981;22(3):257-65. Epub 1981/06/01. PubMed PMID: 6263604.

112. Nakano K, Takahashi S, Mizobuchi M, Kuroda T, Masuda K, Kitoh J. High levels of quinolinic acid in brain of epilepsy-prone E1 mice. Brain research. 1993;619(1-2):195-8. Epub 1993/08/13. PubMed PMID: 8374778.

113. Schwarcz R, Speciale C, Okuno E, French ED, Kohler C. Quinolinic acid: a pathogen in seizure disorders? Advances in experimental medicine and biology. 1986;203:697-707. Epub 1986/01/01. PubMed PMID: 3024466.

114. Curzon G, Bridges PK. Tryptophan metabolism in depression. J Neurol Neurosurg Psychiatry. 1970;33(5):698-704. Epub 1970/10/01. PubMed PMID: 5478953; PMCID: PMC493552.

115. Lapin IP. Kynurenines as probable participants of depression. Pharmakopsychiatr Neuropsychopharmakol. 1973;6(6):273-9. Epub 1973/11/01. doi: 10.1055/s-0028-1094391. PubMed PMID: 4604664.

116. Oxenkrug GF. Tryptophan kynurenine metabolism as a common mediator of genetic and environmental impacts in major depressive disorder: the serotonin hypothesis revisited 40 years later. Isr J Psychiatry Relat Sci. 2010;47(1):56-63. Epub 2010/08/06. PubMed PMID: 20686200; PMCID: PMC3021918.

117. Beratis S, Katrivanou A, Georgiou S, Monastirli A, Pasmatzi E, Gourzis P, Tsambaos D. Major depression and risk of depressive symptomatology associated with short-term and low-dose interferon-alpha treatment. J Psychosom Res. 2005;58(1):15-8. Epub 2005/03/18. doi: 10.1016/j.jpsychores.2004.03.010. PubMed PMID: 15771865.

118. Wichers MC, Koek GH, Robaeys G, Praamstra AJ, Maes M. Early increase in vegetative symptoms predicts IFN-alpha-induced cognitive-depressive changes. Psychological medicine. 2005;35(3):433-41. Epub 2005/04/22. PubMed PMID: 15841878.

119. Capuron L, Neurauter G, Musselman DL, Lawson DH, Nemeroff CB, Fuchs D, Miller AH. Interferon-alpha-induced changes in tryptophan metabolism. relationship to depression and paroxetine treatment. Biol Psychiatry. 2003;54(9):906-14. Epub 2003/10/24. PubMed PMID: 14573318.

120. Wichers MC, Koek GH, Robaeys G, Verkerk R, Scharpe S, Maes M. IDO and interferon-alpha-induced depressive symptoms: a shift in hypothesis from tryptophan depletion to neurotoxicity. Mol Psychiatry. 2005;10(6):538-44. Epub 2004/10/21. doi: 10.1038/sj.mp.4001600. PubMed PMID: 15494706.

121. Lim CK, Essa MM, de Paula Martins R, Lovejoy DB, Bilgin AA, Waly MI, Al-Farsi YM, Al-Sharbati M, Al-Shaffae MA, Guillemin GJ. Altered kynurenine pathway metabolism in autism: Implication for immune-induced glutamatergic activity. Autism Res. 2016;9(6):621-31. Epub 2015/10/27. doi: 10.1002/aur.1565. PubMed PMID: 26497015.

122. Bryn V, Verkerk R, Skjeldal OH, Saugstad OD, Ormstad H. Kynurenine Pathway in Autism Spectrum Disorders in Children. Neuropsychobiology. 2017;76(2):82-8. Epub 2018/04/26. doi: 10.1159/000488157. PubMed PMID: 29694960.

123. Ohja K, Gozal E, Fahnestock M, Cai L, Cai J, Freedman JH, Switala A, El-Baz A, Barnes GN. Neuroimmunologic and Neurotrophic Interactions in Autism Spectrum Disorders: Relationship to Neuroinflammation. Neuromolecular medicine. 2018;20(2):161-73. Epub 2018/04/25. doi: 10.1007/s12017-018-8488-8. PubMed PMID: 29691724; PMCID: PMC5942347.

124. Schwarcz R, Whetsell WO, Jr., Mangano RM. Quinolinic acid: an endogenous metabolite that produces axon-sparing lesions in rat brain. Science. 1983;219(4582):316-8. Epub 1983/01/21. PubMed PMID: 6849138.

125. Costa AC, Scott-McKean JJ, Stasko MR. Acute injections of the NMDA receptor antagonist memantine rescue performance deficits of the Ts65Dn mouse model of Down syndrome on a fear conditioning test. Neuropsychopharmacology. 2008;33(7):1624-32. Epub 2007/08/19. doi: 10.1038/sj.npp.1301535. PubMed PMID: 17700645.

126. Lockrow J, Boger H, Bimonte-Nelson H, Granholm AC. Effects of long-term memantine on memory and neuropathology in Ts65Dn mice, a model for Down syndrome. Behav Brain Res. 2011;221(2):610-22. doi: 10.1016/j.bbr.2010.03.036. PubMed PMID: 20363261; PMCID: PMC2928411.

127. Scott-McKean JJ, Costa AC. Exaggerated NMDA mediated LTD in a mouse model of Down syndrome and pharmacological rescuing by memantine. Learn Mem. 2011;18(12):774-8. Epub 2011/11/22. doi: 10.1101/lm.024182.111. PubMed PMID: 22101180; PMCID: PMC3222894.

128. Ahmed MM, Dhanasekaran AR, Block A, Tong S, Costa AC, Gardiner KJ. Protein profiles associated with context fear conditioning and their modulation by memantine. Mol Cell Proteomics. 2014;13(4):919-37. doi: 10.1074/mcp.M113.035568. PubMed PMID: 24469516; PMCID: PMC3977192.

129. Victorino DB, Bederman IR, Costa ACS. Pharmacokinetic Properties of Memantine after a Single Intraperitoneal Administration and Multiple Oral Doses in Euploid Mice and in the Ts65Dn Mouse Model of Down's Syndrome. Basic Clin Pharmacol Toxicol. 2017;121(5):382-9. Epub 2017/05/31. doi: 10.1111/bcpt.12816. PubMed PMID: 28557265.

130. Boada R, Hutaff-Lee C, Schrader A, Weitzenkamp D, Benke TA, Goldson EJ, Costa AC. Antagonism of NMDA receptors as a potential treatment for Down syndrome: a pilot randomized controlled trial. Transl

Psychiatry. 2012;2:e141. Epub 2012/07/19. doi: 10.1038/tp.2012.66. PubMed PMID: 22806212; PMCID: PMC3410988.

131. Hanney M, Prasher V, Williams N, Jones EL, Aarsland D, Corbett A, Lawrence D, Yu LM, Tyrer S, Francis PT, Johnson T, Bullock R, Ballard C, researchers Mt. Memantine for dementia in adults older than 40 years with Down's syndrome (MEADOWS): a randomised, double-blind, placebo-controlled trial. Lancet. 2012;379(9815):528-36. Epub 2012/01/13. doi: 10.1016/S0140-6736(11)61676-0. PubMed PMID: 22236802.

132. Koblish HK, Hansbury MJ, Bowman KJ, Yang G, Neilan CL, Haley PJ, Burn TC, Waeltz P, Sparks RB, Yue EW, Combs AP, Scherle PA, Vaddi K, Fridman JS. Hydroxyamidine inhibitors of indoleamine-2,3-dioxygenase potently suppress systemic tryptophan catabolism and the growth of IDO-expressing tumors. Mol Cancer Ther. 2010;9(2):489-98. Epub 2010/02/04. doi: 10.1158/1535-7163.MCT-09-0628. PubMed PMID: 20124451.

133. Stone TW, Darlington LG. The kynurenine pathway as a therapeutic target in cognitive and neurodegenerative disorders. Br J Pharmacol. 2013;169(6):1211-27. Epub 2013/05/08. doi: 10.1111/bph.12230. PubMed PMID: 23647169; PMCID: PMC3831703.

134. Roskoski R, Jr. Janus kinase (JAK) inhibitors in the treatment of inflammatory and neoplastic diseases. Pharmacological research. 2016;111:784-803. doi: 10.1016/j.phrs.2016.07.038. PubMed PMID: 27473820.

135. Fritz-French C, Shawahna R, Ward JE, Maroun LE, Tyor WR. The recombinant vaccinia virus gene product, B18R, neutralizes interferon alpha and alleviates histopathological complications in an HIV encephalitis mouse model. Journal of interferon & cytokine research : the official journal of the International Society for Interferon and Cytokine Research. 2014;34(7):510-7. doi: 10.1089/jir.2013.0072. PubMed PMID: 24564363; PMCID: 4080846.

136. Mandi Y, Vecsei L. The kynurenine system and immunoregulation. Journal of neural transmission. 2012;119(2):197-209. Epub 2011/07/12. doi: 10.1007/s00702-011-0681-y. PubMed PMID: 21744051.

137. Alberati-Giani D, Ricciardi-Castagnoli P, Kohler C, Cesura AM. Regulation of the kynurenine metabolic pathway by interferon-gamma in murine cloned macrophages and microglial cells. Journal of neurochemistry. 1996;66(3):996-1004. Epub 1996/03/01. PubMed PMID: 8769859.

138. Englund A, Jonsson B, Zander CS, Gustafsson J, Anneren G. Changes in mortality and causes of death in the Swedish Down syndrome population. American journal of medical genetics Part A. 2013;161A(4):642-9. Epub 2013/02/26. doi: 10.1002/ajmg.a.35706. PubMed PMID: 23436430.

139. Nemkov T, Hansen KC, D'Alessandro A. A three-minute method for high-throughput quantitative metabolomics and quantitative tracing experiments of central carbon and nitrogen pathways. Rapid Commun Mass Spectrom. 2017;31(8):663-73. Epub 2017/02/15. doi: 10.1002/rcm.7834. PubMed PMID: 28195377; PMCID: PMC5364945.

140. Nemkov T, Sun K, Reisz JA, Song A, Yoshida T, Dunham A, Wither MJ, Francis RO, Roach RC, Dzieciatkowska M, Rogers SC, Doctor A, Kriebardis A, Antonelou M, Papassideri I, Young CT, Thomas TA, Hansen KC, Spitalnik SL, Xia Y, Zimring JC, Hod EA, D'Alessandro A. Hypoxia modulates the purine salvage pathway and decreases red blood cell and supernatant levels of hypoxanthine during refrigerated storage. Haematologica. 2018;103(2):361-72. Epub 2017/10/29. doi: 10.3324/haematol.2017.178608. PubMed PMID: 29079593; PMCID: PMC5792281.

141. Clasquin MF, Melamud E, Rabinowitz JD. LC-MS data processing with MAVEN: a metabolomic analysis and visualization engine. Curr Protoc Bioinformatics. 2012;Chapter 14:Unit14 1. Epub 2012/03/06. doi: 10.1002/0471250953.bi1411s37. PubMed PMID: 22389014; PMCID: PMC4055029.

142. Melamud E, Vastag L, Rabinowitz JD. Metabolomic analysis and visualization engine for LC-MS data. Anal Chem. 2010;82(23):9818-26. Epub 2010/11/06. doi: 10.1021/ac1021166. PubMed PMID: 21049934; PMCID: PMC5748896.

143. Benjamini Y, Hochberg Y. Controlling the False Discovery Rate - a Practical and Powerful Approach to Multiple Testing. Journal of the Royal Statistical Society Series B-Methodological. 1995;57(1):289-300. PubMed PMID: ISI:A1995QE45300017.

144. Tenenbaum D. KEGGREST: Client-side REST access to KEGG. 1.20.0 ed2018. p. R package.

145. Hastie T, Tibshirani R, Narasimhan B, Chu G. Impute: Imputation for microarray data 1.52.0 ed2017. p. R Package.

146. Friedman J, Hastie T, Tibshirani R. Regularization Paths for Generalized Linear Models via Coordinate Descent. J Stat Softw. 2010;33(1):1-22. Epub 2010/09/03. PubMed PMID: 20808728; PMCID: PMC2929880.

FIGURE LEGENDS.

Table 1 – Demographic characteristics of study participants in Cohort 1 and Cohort 2.

Figure 1 – Trisomy 21 causes consistent changes in circulating metabolite abundance.

A) Differentially abundant metabolites in plasma samples from individuals with T21 were identified using a linear model adjusting for age, sex, and cohort. Metabolites that increased in the T21 group are shown in red and metabolites that decreased in the T21 group are blue. The horizontal grey line represents an adjusted p-value of 0.01. **B)** Box plots showing model residuals (i.e. remaining component of the model fit after adjusting for age, sex, and cohort) for significantly differentially abundant metabolites. p-values were calculated using the linear model from **A** and Benjamini-Hochberg for multiple testing correction. **C)** Top 5 most significant KEGG pathways identified by enrichment analysis. Each of the 91 metabolites analyzed is ranked by fold change, with blue and red lines indicating a pathway metabolite significantly down- or up-regulated in the T21 group, respectively. Grey lines indicate that a pathway metabolite was not significantly differentially altered. p-values were calculated using a hypergeometric test and Benjamini-Hochberg correction was used to adjust the p-values. The numbers of significant (sig) and total of the 91 metabolites present in each KEGG pathway are shown to the right.

Figure 1 – figure supplement 1 – Statistical workflow adjusts for the effects of age and sex in circulating plasma metabolites.

A) Overview of the analysis pipeline used to identify, annotate, and analyze plasma metabolites measured in individuals with Down syndrome (T21 group) and controls without Down syndrome (D21) from the Translational Nexus Biobank (Nexus, Cohort 1) and the Human Trisome Project (HTP, Cohort 2). Putative metabolites were annotated using MAVEN. Across the two cohorts, 97 metabolites were detected consistently. Data preprocessing included filtering out metabolites with low intensity values or that were detected in less than 90% of the T21 and/or D21 samples, leaving 91 metabolites. Batch correction and linear model fitting was performed before the combined data set was used for analysis. **B)** Differentially abundant metabolites in plasma samples from T21 individuals in Cohort 1 alone. Metabolites that increased in the T21 group are shown in red and metabolites that decreased in the T21 group are blue. The horizontal grey line represents an adjusted p-value of 0.01 estimated using a linear model fit with no covariates (left) or including age and sex as covariates (right). **C)** Differentially abundant metabolites in plasma samples from T21 individuals in Cohort 2 alone, colored as described in **B**. The horizontal grey line represents a Benjamini-Hochberg adjusted p-value of 0.01 estimated using a linear model fit with no covariates (left) or including age and sex as covariates (right).

Figure 1 – figure supplement 2 – Adjustment for age and sex covariates prior to metabolomics analyses.

A) Density plots showing the distribution of $\log_2$ intensity values for all 91 metabolites in Cohort 1 (purple) and Cohort 2 (green) prior to any adjustment. **B)** Density plots showing the distribution of adjusted $\log_2$ intensity values for all 91 metabolites, colored as in **A**, after a linear model was used to adjust for age, sex, and cohort covariates. **C)** Principal components plot showing each sample in the Cohort 1 and Cohort 2, colored as in **A** and **B**. Triangle and circle points represent T21 and D21 individuals, respectively. The first and second principal components representing all 91 metabolites are plotted, with their respective percentage of variance explained

shown in parentheses. **D**) Principal components plot as in **C**, after data for the 91 metabolites had been adjusted for age, sex, and cohort.

Figure 2 – A signature of tryptophan catabolites and inflammation-related metabolites accurately distinguishes plasma samples from individuals with trisomy 21.

A) Receiver operating characteristic (ROC) plot reporting the area under the curve (AUC) for each of the 16 significantly differentially abundant metabolites. **B)** Box and whisker plots showing the distribution of lasso regression coefficients for the 11 metabolites selected in 80% of models meeting accuracy > 90% over 10,000 bootstrapped iterations. **C)** Bootstrapped, multivariate model performance using the selected 11 metabolites from **B** across 10,000 iterations. The mean internally cross-validated result with 95% confidence intervals are shown.

Figure 3 – Trisomy 21 induces the kynurenine pathway. Schematic of tryptophan metabolism and the kynurenine pathway. Metabolite levels are plotted as model residuals (i.e. remaining component of the model fit after adjusting for age, sex, and cohort). p-values were calculated using the linear model from **Figure 1A** Benjamini-Hochberg for multiple testing correction Multi-headed arrows are used to represent multiple steps in the pathway that are not shown. Arrows with dashed lines represent reactions occurring in tryptophanase-expressing gastrointestinal microbiota.

Figure 3 – figure supplement 1 – Individuals with Down syndrome have elevated kynurenine/tryptophan, quinolinic acid/picolinic acid, and quinolinic acid/kynurenic acid ratios. A) The levels of kynurenic acid (only detected in the Cohort 1 HTP plasma samples) were not significantly altered in T21 individuals after adjusting for age and sex. The ratios of **B)** kynurenine to tryptophan and **C)** quinolinic acid to picolinic acid were significantly increased in T21 individuals by a Benjamini-Hochberg adjusted p-value < 0.01. **D)** The ratio of quinolinic acid to kynurenic acid was moderately increased in T21 individuals (adjusted p = 0.04).

Figure 3 – figure supplement 2 – Metabolites involved in microbiome-mediated tryptophan synthesis in people with and without trisomy 21.

Simplified schematic of tryptophan synthesis. Box and whisker plots showing model residuals (i.e. remaining component of the model fit after adjusting for, age, sex, and cohort), for which metabolites that increased in the T21 group are shown in red and metabolites that decreased in the T21 group are shown in blue. P-values were calculated using the linear model in **Figure 1A** adjusting for cohort, with age and sex as covariates, and using Benjamini-Hochberg for multiple testing correction.

Figure 4 – Trisomy 21 sensitizes cells to super-induction of the kynurenine pathway by IFN-α.

Flux metabolomics experiment using heavy-labeled tryptophan in fibroblast cell lines (n = 3 T21, n = 3 D21). **A)** Levels of heavy-labeled tryptophan in D21 (left) and T21 (right) fibroblast cell lysates, with or without IFN-α treatment. **B)** Levels of heavy-labeled kynurenine in D21 (left) and T21 (right) supernatant, with or without IFN-α treatment. **C)** Ratio of heavy-labeled kynurenine to heavy-labeled tryptophan levels in D21 (left) and T21 (right) supernatant, with or without IFN-α treatment. At each timepoint, the p-value between the Ctrl and IFN+ samples

was calculated using a two-tailed student's t-test and Benjamini-Hochberg for multiple testing correction (* $p < 0.05$, ** $p < 0.01$, *** $p < 0.001$). **D)** Western blot analysis confirming STAT1 phosphorylation and upregulation of IDO1 over a 24 hour timecourse. **E)** Western blot analysis confirming STAT1 phosphorylation all six cell lines and IDO1 super-induction in T21 fibroblasts after 24 hours of IFN-α treatment.

Figure 4 – figure supplement 1 – Trisomy 21 sensitizes cells to super-induction of the kynurenine pathway by IFN-α.

Flux metabolomics experiment using heavy-labeled tryptophan in fibroblast cell lines (n = 3 T21, n = 3 D21). **A)** Levels of heavy-labeled tryptophan in D21 (left) and T21 (right) supernatant, with or without IFN-α treatment. **B)** Levels of heavy-labeled kynurenine in D21 (left) and T21 (right) fibroblast cell lysates, with or without IFN-α treatment. **C)** Ratio of heavy-labeled kynurenine to heavy-labeled tryptophan levels in D21 (left) and T21 (right) fibroblast cell lysates, with or without IFN-α treatment. At each timepoint, the p-value between the Ctrl and IFN+ samples was calculated using a two-tailed student's t-test and Benjamini-Hochberg for multiple testing correction (* $p < 0.05$, ** $p < 0.01$, *** $p < 0.001$).

Figure 5 - Tryptophan catabolism is disrupted in the *Dp(16)1/Yey* mouse model of DS.

A) Box and whisker plots showing levels of plasma kynurenine in the indicated mouse model. **B)** Box and whisker plots showing levels of plasma kynurenine in WT and Dp16 mice injected with sham or poly(I:C). p-values were calculated using a two-tailed student's t-test (* $p < 0.05$).

Figure 6 – Kynurenine dysregulation positively correlates with circulating levels of IFN-α and IFN-inducible cytokines.

A) Heatmap showing ranked Spearman's correlation values between kynurenine and a panel of cytokines measured by a Mesoscale Discovery (MSD) assay. **B, C)** Scatterplots for the two cytokines most positively correlated (Spearman's correlation) with kynurenine, IFN-α2a and MCP-1, are shown to the right, with points in red and black representing T21 and D21 samples, respectively. **D)** Heatmap showing ranked Spearman's correlations between quinolinic acid and cytokines measured by the MSD assay. **E, F)** Scatterplots for the two cytokines most positively correlated (Spearman's correlation) with quinolinic acid, MCP-1 and MCP-4, are shown to the right, with points in red and black representing T21 and D21 samples, respectively.

Supplemental File 1. Metabolomics Data. A) Plasma Metabolomics **B)** KEGG Analysis **C)** Flux experiment.

Characteristics	Cohort		Combined
	1 - Nexus (n = 98)	2 - HTP (n = 71)	COMBINED (n = 169)
Karyotype			
Euploid (D21)	49 (50.0%)	41 (57.7%)	90 (53.3%)
Trisomy 21 (T21)	49 (50.0%)	30 (42.3%)	79 (46.7%)
Age, All			
0-18	68 (69.4%)	7 (9.9%)	75 (44.4%)
19-30	13 (13.3%)	28 (39.4%)	41 (24.3%)
31-65	17 (17.3%)	36 (50.7%)	53 (31.4%)
Age, D21			
0-18	24	4	28
19-30	8	13	21
31-65	17	24	41
Age, T21			
0-18	44	3	47
19-30	5	15	20
31-65	0	12	12
Sex, All			
Male	44 (44.9%)	27 (38.0%)	71 (42.0%)
Female	54 (55.1%)	44 (62.0%)	98 (58.0%)
Sex, D21			
Male	18	15	33
Female	31	26	57
Sex, T21			
Male	26	12	38
Female	23	18	41

D21 = euploid chr21, T21 = trisomic chr21. Data shown as n (%).

Table 1. Baseline characteristics of the cohorts from which plasma samples were obtained.

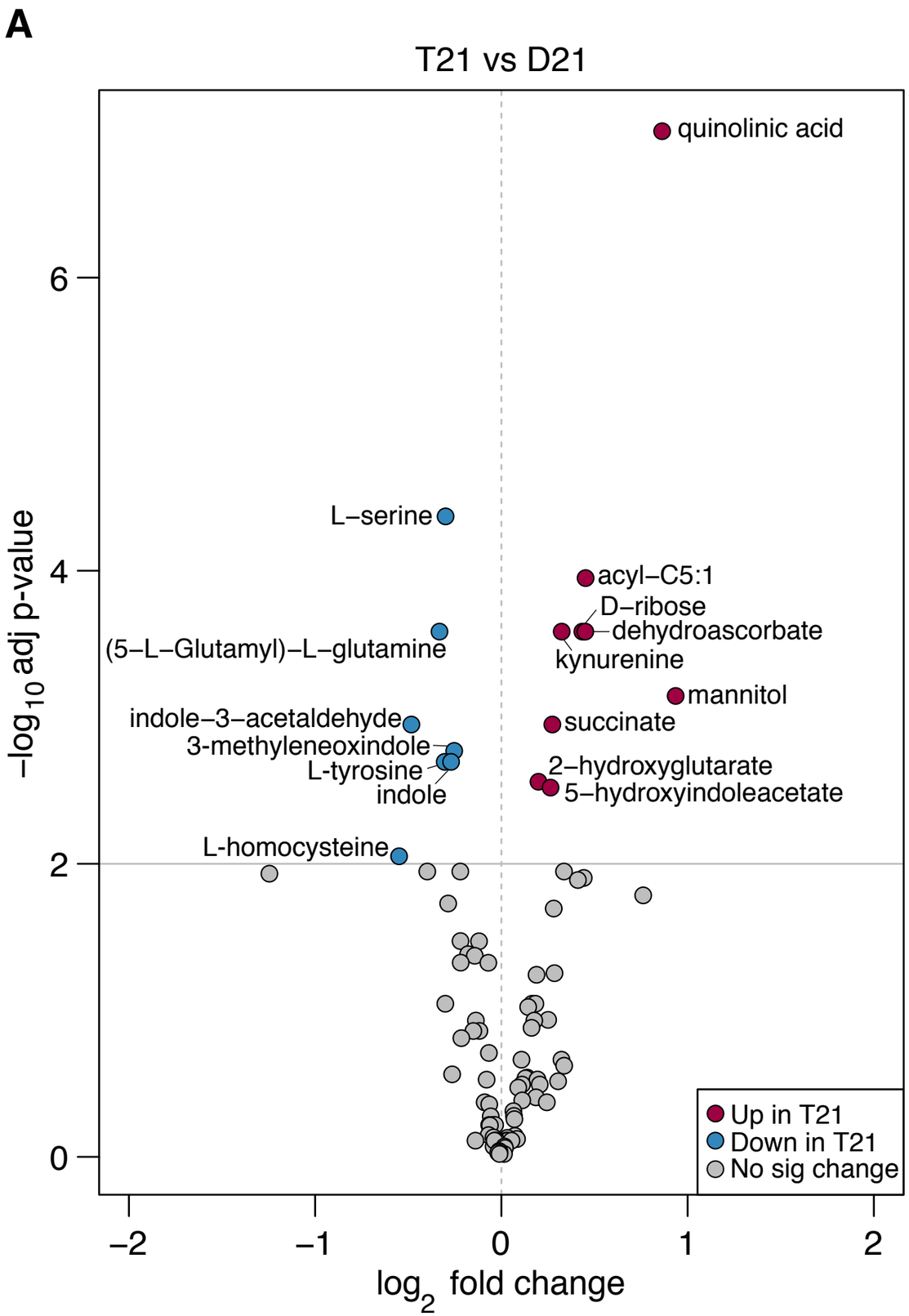
A
T21 vs D21
quinolinic acid
L–serine
acyl–C5:1
D–ribose
dehydroascorbate
(5–L–Glutamyl)–L–glutamine
kynurenine
mannitol
indole–3–acetaldehyde
succinate
3-methyleneoxindole
2–hydroxyglutarate
L-tyrosine
5–hydroxyindoleacetate
indole
L-homocysteine
Up in T21
Down in T21
No sig change
−log10 adj p-value
log2 fold change

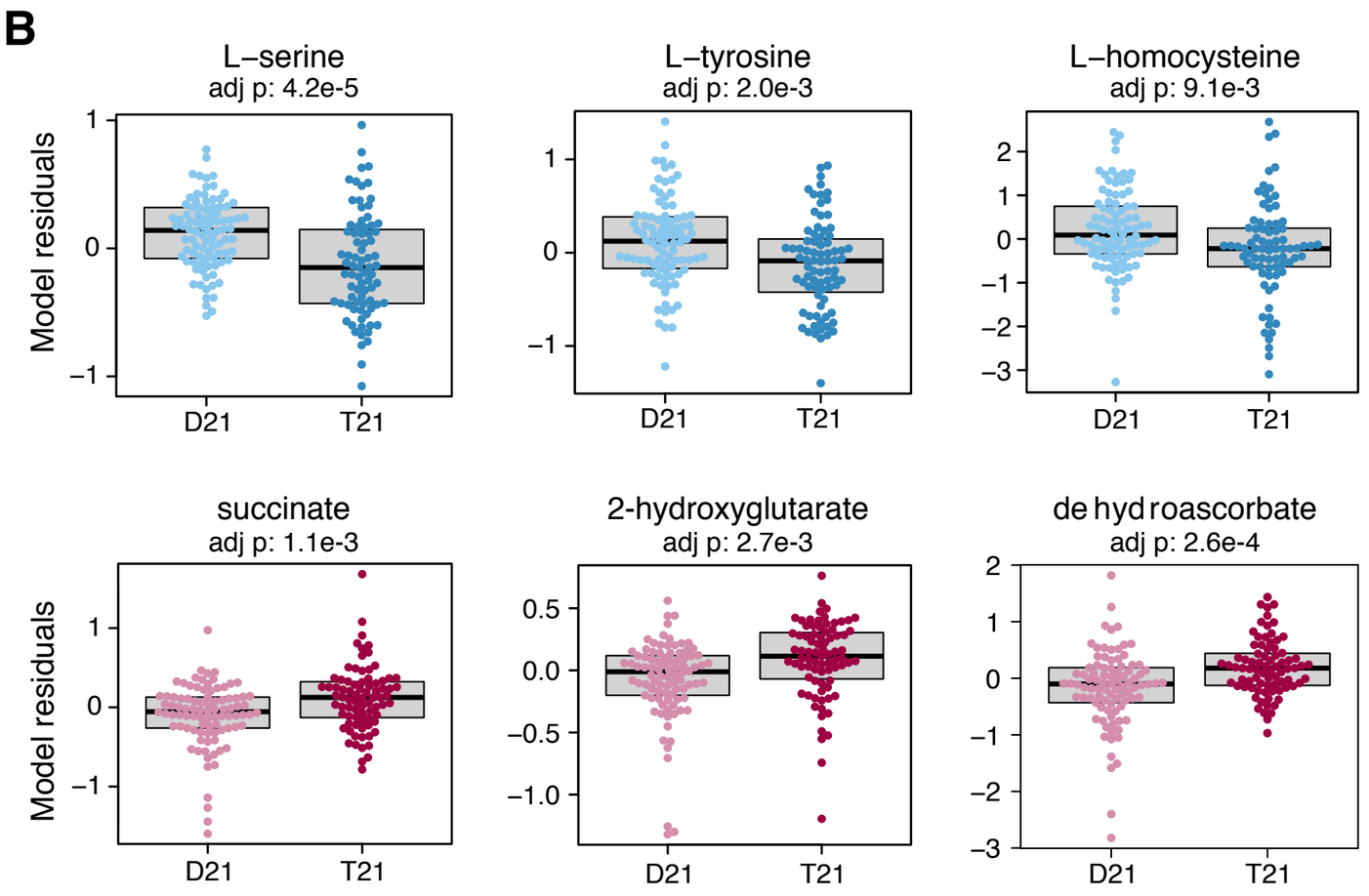
B
L–serine
adj p: 4.2e-5
L–tyrosine
adj p: 2.0e-3
L–homocysteine
adj p: 9.1e-3
succinate
adj p: 1.1e-3
2-hydroxyglutarate
adj p: 2.7e-3
de hyd roascorbate
adj p: 2.6e-4
Model residuals
D21
T21

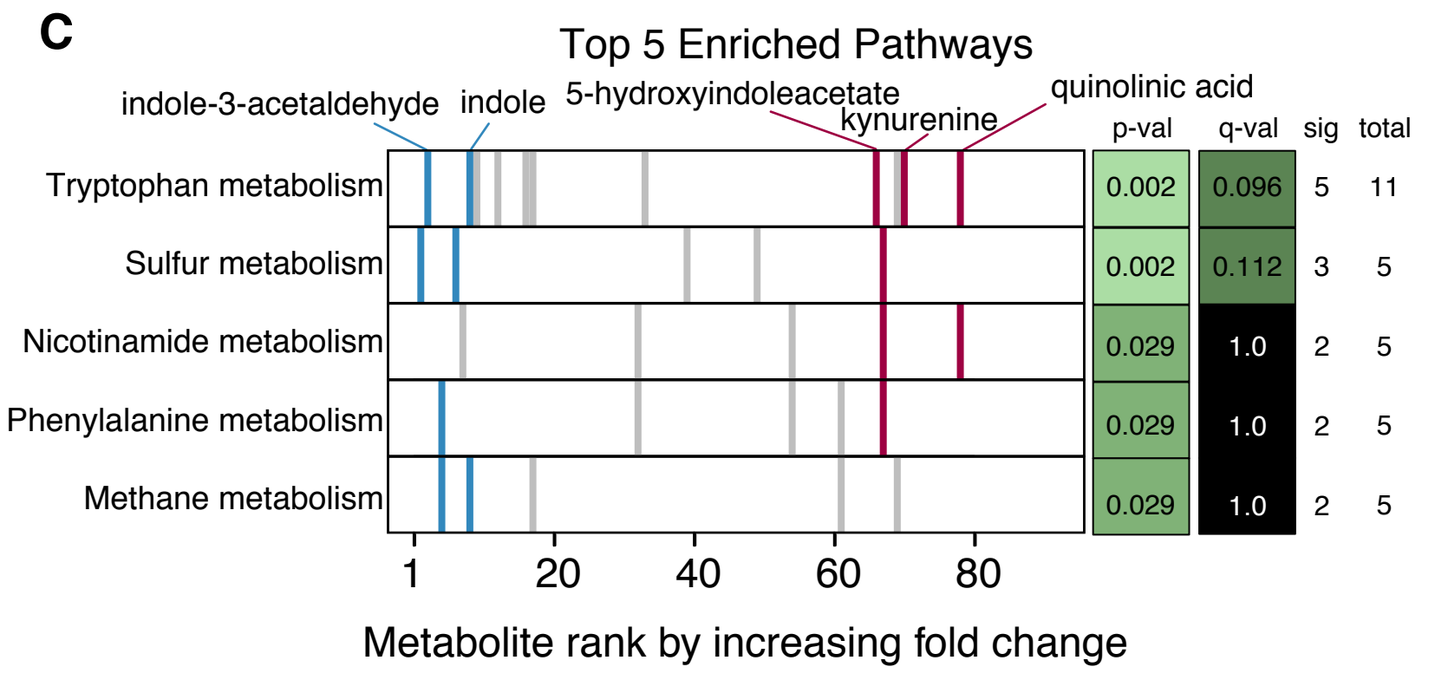
C
Top 5 Enriched Pathways
indole-3-acetaldehyde
indole
5-hydroxyindoleacetate
kynurenine
quinolinic acid
p-val
q-val
sig
total
Tryptophan metabolism
0.002
0.096
5
11
Sulfur metabolism
0.002
0.112
3
5
Nicotinamide metabolism
0.029
1.0
2
5
Phenylalanine metabolism
0.029
1.0
2
5
Methane metabolism
0.029
1.0
2
5
Metabolite rank by increasing fold change

Powers et al., Figure 1 - figure supplement 1

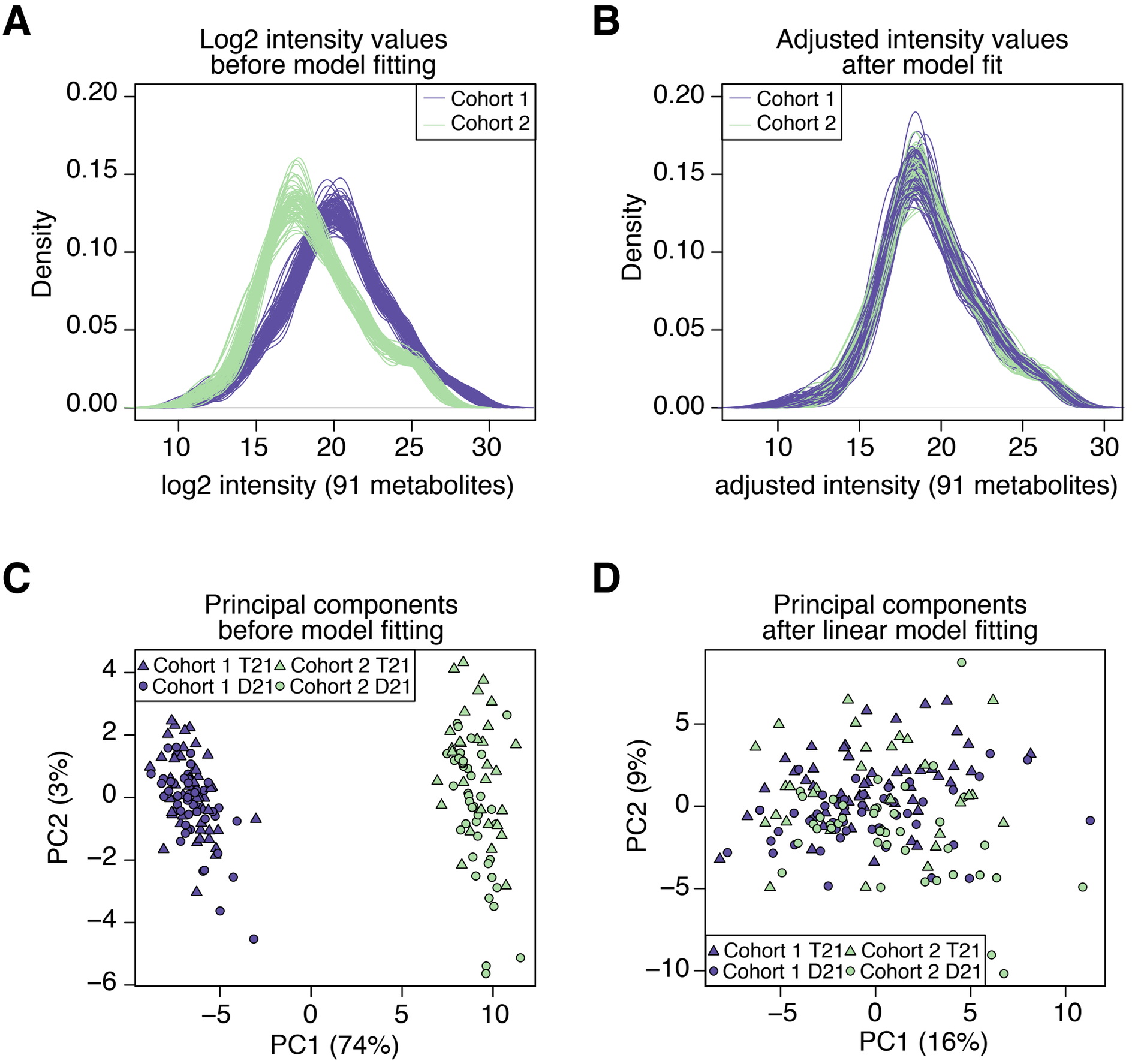
A
Log2 intensity values
before model fitting
Density
0.20
0.15
0.10
0.05
0.00
Cohort 1
Cohort 2
10
15
20
25
30
log2 intensity (91 metabolites)
B
Adjusted intensity values
after model fit
Density
0.20
0.15
0.10
0.05
0.00
Cohort 1
Cohort 2
10
15
20
25
30
adjusted intensity (91 metabolites)
C
Principal components
before model fitting
PC2 (3%)
4
2
0
−2
−4
−6
Cohort 1 T21
Cohort 2 T21
Cohort 1 D21
Cohort 2 D21
−5
0
5
10
PC1 (74%)
D
Principal components
after linear model fitting
PC2 (9%)
5
0
−5
−10
Cohort 1 T21
Cohort 2 T21
Cohort 1 D21
Cohort 2 D21
−5
0
5
10
PC1 (16%)

Powers et al., Figure 2

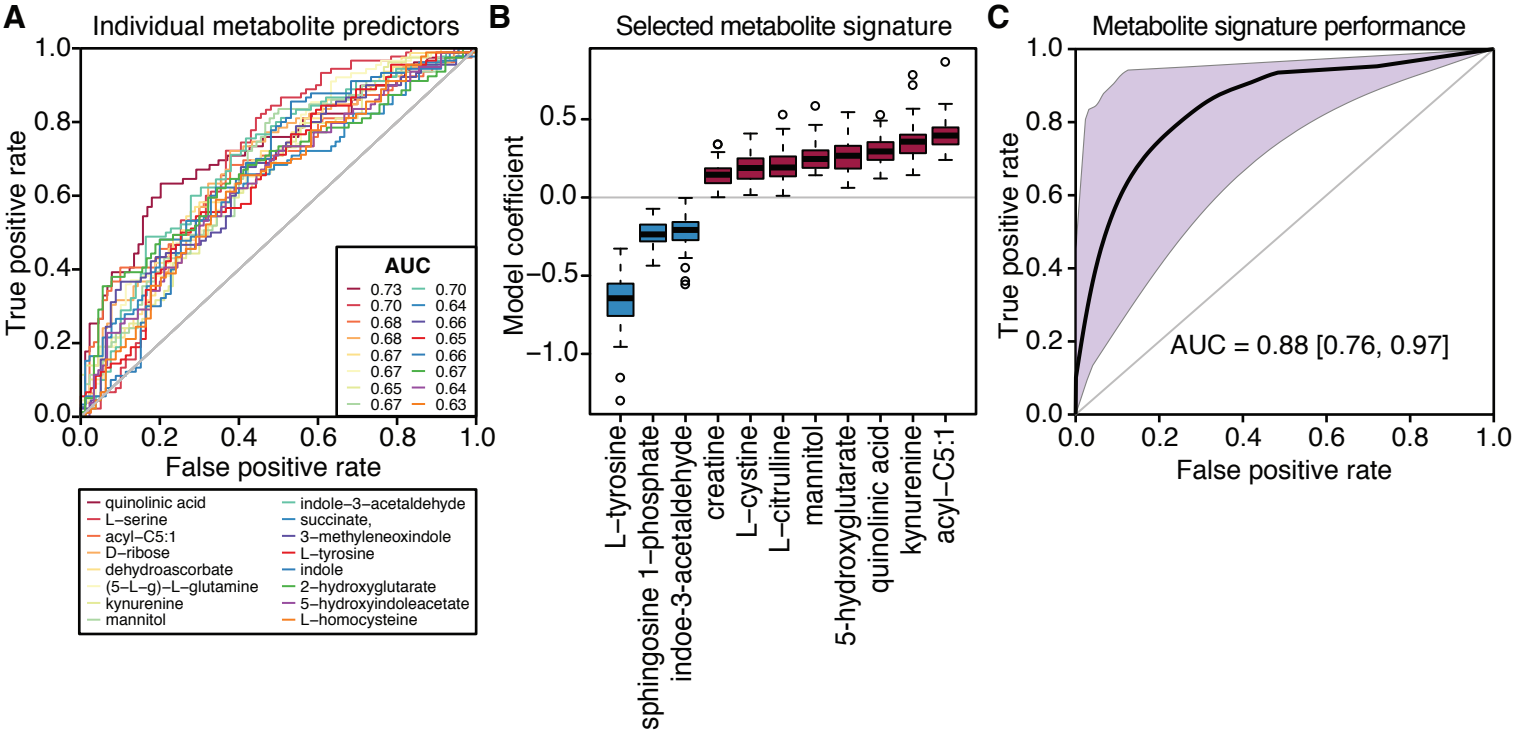

serotonin
n.s.

L-tryptophan
n.s.

indole
adj p: 2.0e-3

5-hydroxyindoleacetate
adj p: 3.0e-3

indole-3-acetaldehyde
adj p: 1.1e-3

kynurenine
adj p: 2.6e-4

indole-3-acetate
n.s

anthranilate
n.s.

quinolinic acid
adj p: 1.0e-7

gamma-oxalo-
crotonate
n.s.

picolinic acid
n.s.

Model residuals

D21

T21

serotonin

L-tryptophan

indole

IDO1, IDO2
TDO2

5-hydroxyindoleacetate
(5-HIA)

N-formylkynurenine

indole-3-acetaldehyde

kynurenine

indole-3-acetate

3-hydroxykynurenine

anthranilate

2-amino-3-carboxymuconate
semialdehyde

- Significantly up-regulated in T21
- Significantly down-regulated in T21
- Not significantly different

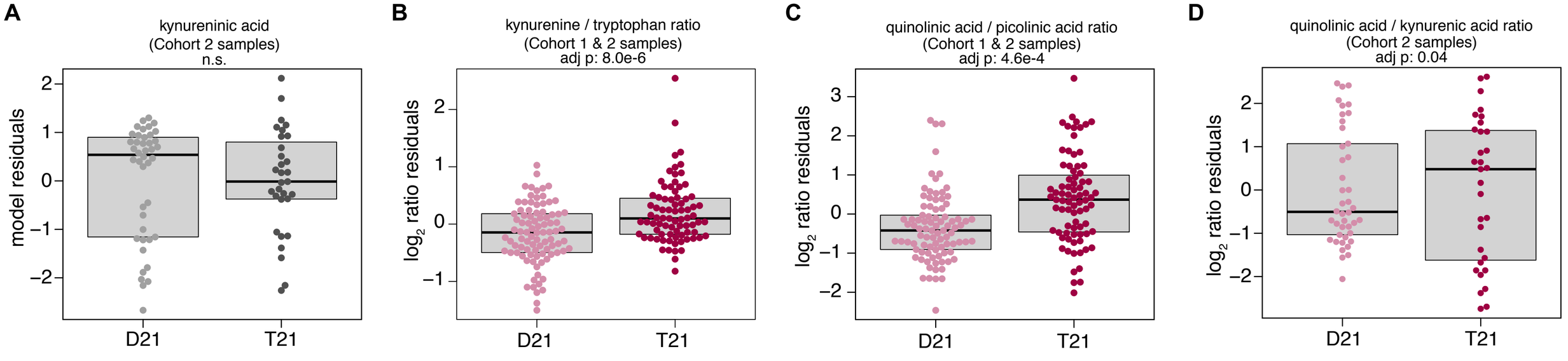
A
kynureninic acid
(Cohort 2 samples)
n.s.
model residuals
2
1
0
−1
−2
D21
T21
B
kynurenine / tryptophan ratio
(Cohort 1 & 2 samples)
adj p: 8.0e-6
log2 ratio residuals
2
1
0
−1
D21
T21
C
quinolinic acid / picolinic acid ratio
(Cohort 1 & 2 samples)
adj p: 4.6e-4
log2 ratio residuals
3
2
1
0
−1
−2
D21
T21
D
quinolinic acid / kynurenic acid ratio
(Cohort 2 samples)
adj p: 0.04
log2 ratio residuals
2
1
0
−1
−2
D21
T21

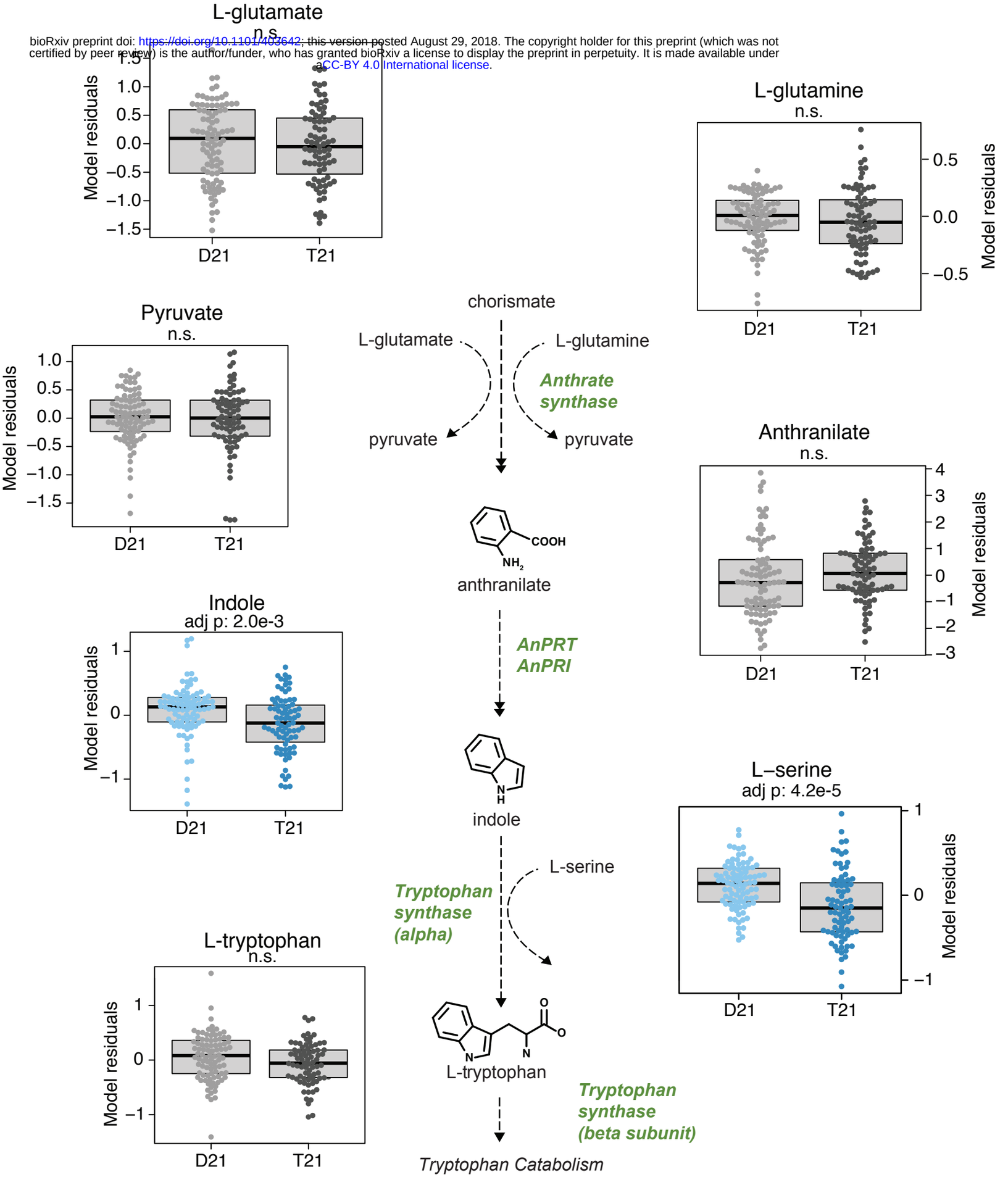

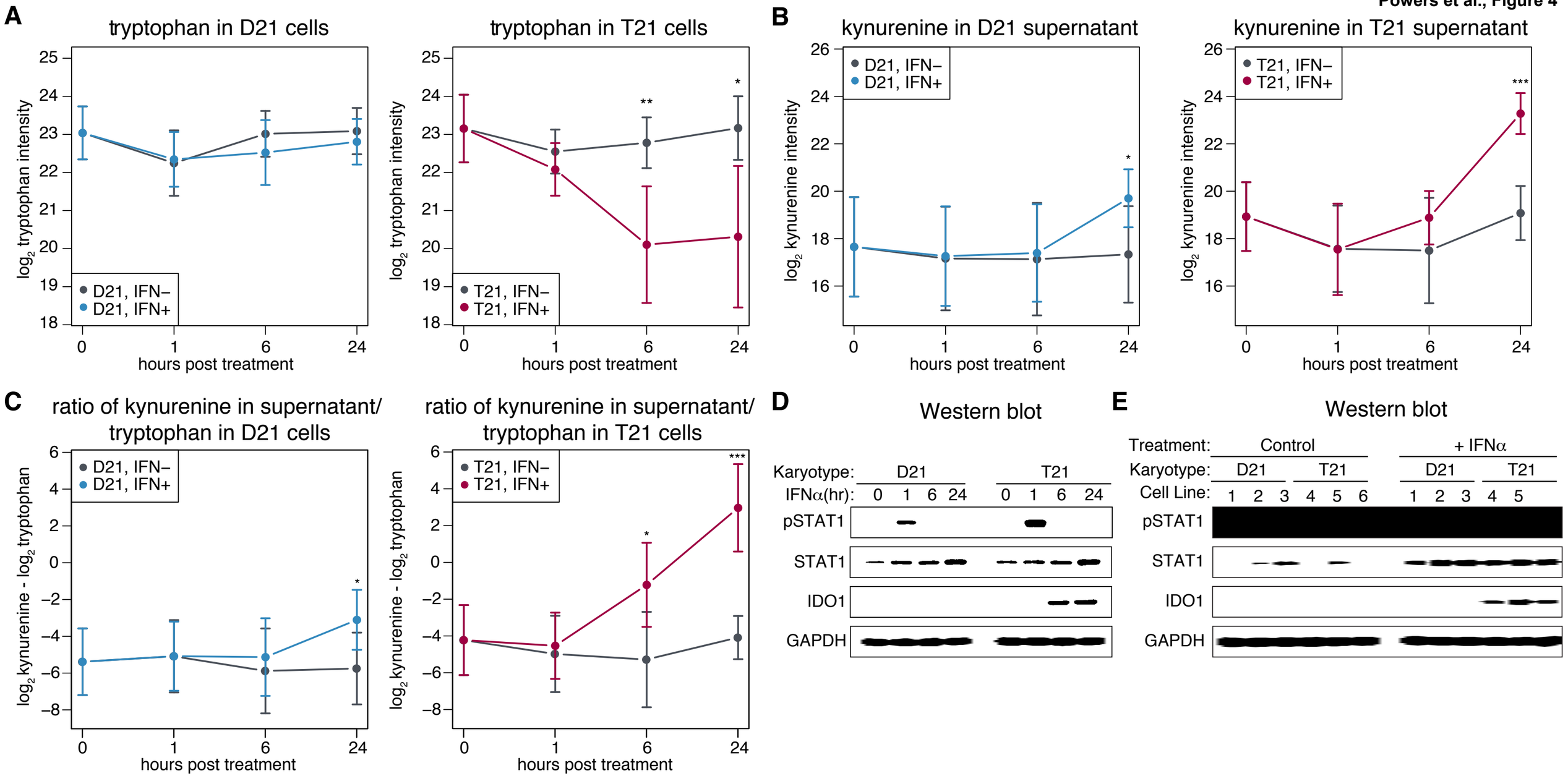
A
tryptophan in D21 cells
log2 tryptophan intensity
D21, IFN–
D21, IFN+
hours post treatment
tryptophan in T21 cells
T21, IFN–
T21, IFN+
B
kynurenine in D21 supernatant
log2 kynurenine intensity
kynurenine in T21 supernatant
C
ratio of kynurenine in supernatant/ tryptophan in D21 cells
log2 kynurenine - log2 tryptophan
ratio of kynurenine in supernatant/ tryptophan in T21 cells
D
Western blot
Karyotype: D21 T21
IFNα(hr): 0 1 6 24 0 1 6 24
pSTAT1
STAT1
IDO1
GAPDH
E
Western blot
Treatment: Control + IFNα
Karyotype: D21 T21 D21 T21
Cell Line: 1 2 3 4 5 6 1 2 3 4 5

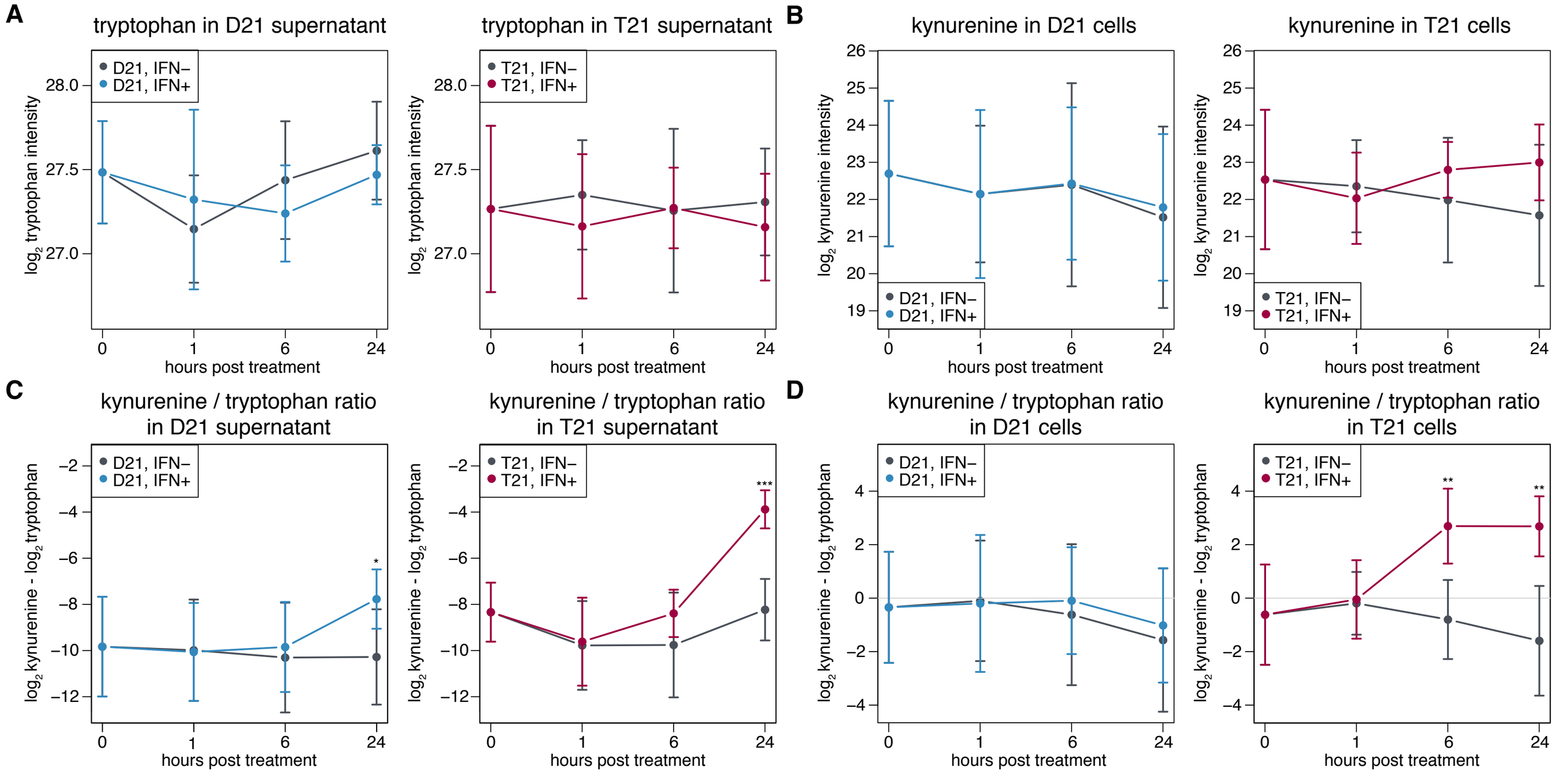
A
tryptophan in D21 supernatant
tryptophan in T21 supernatant
B
kynurenine in D21 cells
kynurenine in T21 cells
C
kynurenine / tryptophan ratio in D21 supernatant
kynurenine / tryptophan ratio in T21 supernatant
D
kynurenine / tryptophan ratio in D21 cells
kynurenine / tryptophan ratio in T21 cells
D21, IFN−
D21, IFN+
T21, IFN−
T21, IFN+
log2 tryptophan intensity
log2 kynurenine intensity
log2 kynurenine - log2 tryptophan
hours post treatment
0
1
6
24
*
**
***

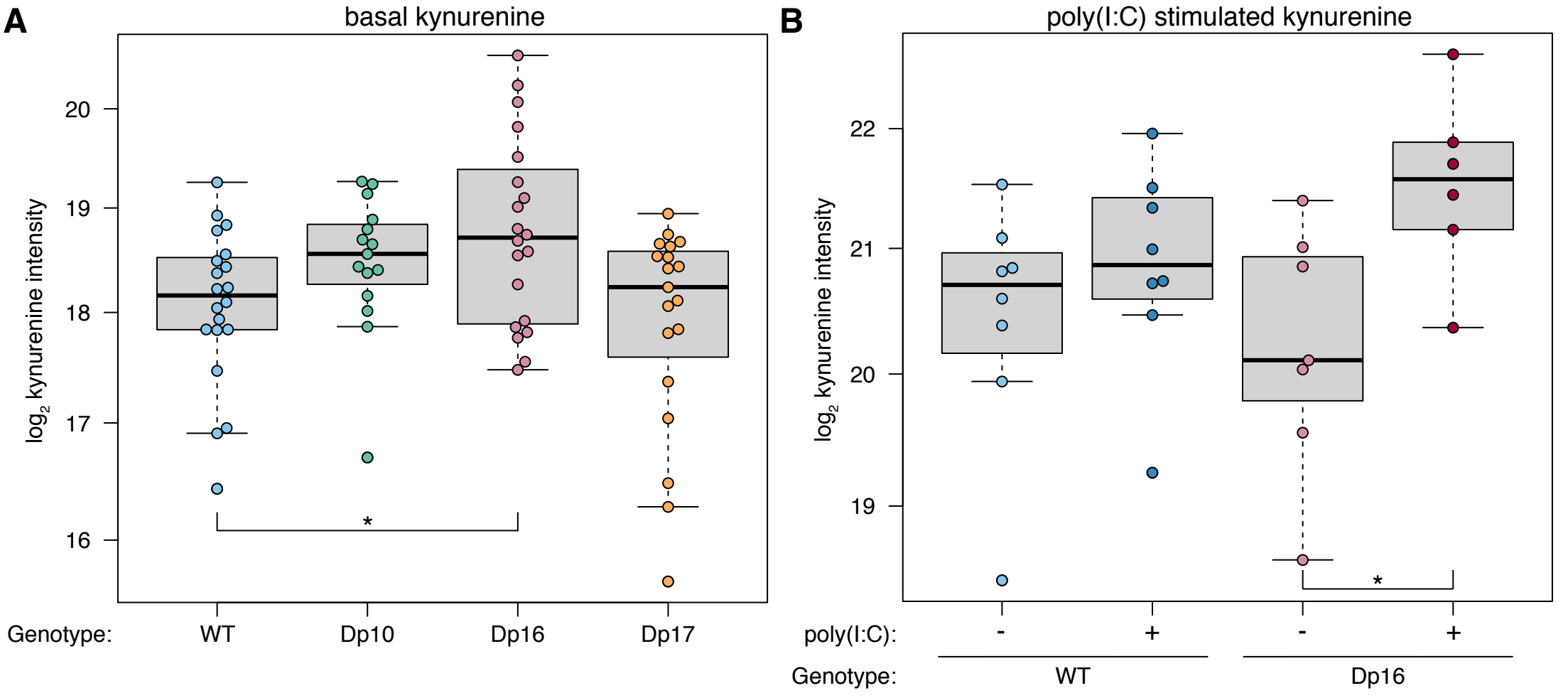
A
basal kynurenine
log2 kynurenine intensity
20
19
18
17
16
*
Genotype:
WT
Dp10
Dp16
Dp17
B
poly(I:C) stimulated kynurenine
log2 kynurenine intensity
22
21
20
19
*
poly(I:C):
-
+
-
+
Genotype:
WT
Dp16

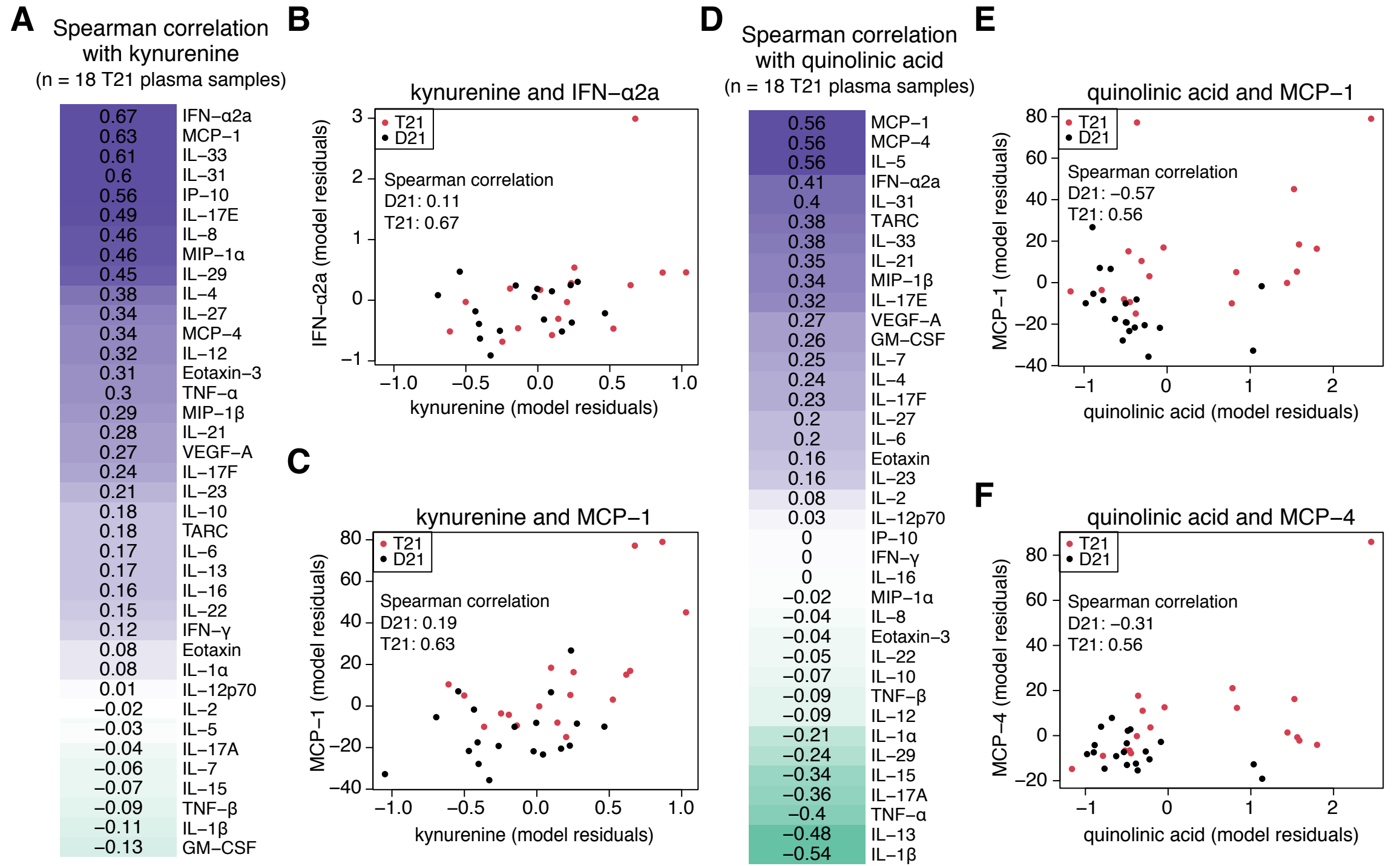
A
Spearman correlation with kynurenine
(n = 18 T21 plasma samples)
0.67 IFN–α2a
0.63 MCP–1
0.61 IL–33
0.6 IL–31
0.56 IP–10
0.49 IL–17E
0.46 IL–8
0.46 MIP–1α
0.45 IL–29
0.38 IL–4
0.34 IL–27
0.34 MCP–4
0.32 IL–12
0.31 Eotaxin–3
0.3 TNF–α
0.29 MIP–1β
0.28 IL–21
0.27 VEGF–A
0.24 IL–17F
0.21 IL–23
0.18 IL–10
0.18 TARC
0.17 IL–6
0.17 IL–13
0.16 IL–16
0.15 IL–22
0.12 IFN–γ
0.08 Eotaxin
0.08 IL–1α
0.01 IL–12p70
–0.02 IL–2
–0.03 IL–5
–0.04 IL–17A
–0.06 IL–7
–0.07 IL–15
–0.09 TNF–β
–0.11 IL–1β
–0.13 GM–CSF
B
kynurenine and IFN–α2a
T21
D21
Spearman correlation
D21: 0.11
T21: 0.67
IFN–α2a (model residuals)
kynurenine (model residuals)
C
kynurenine and MCP–1
T21
D21
Spearman correlation
D21: 0.19
T21: 0.63
MCP–1 (model residuals)
kynurenine (model residuals)
D
Spearman correlation with quinolinic acid
(n = 18 T21 plasma samples)
0.56 MCP–1
0.56 MCP–4
0.56 IL–5
0.41 IFN–α2a
0.4 IL–31
0.38 TARC
0.38 IL–33
0.35 IL–21
0.34 MIP–1β
0.32 IL–17E
0.27 VEGF–A
0.26 GM–CSF
0.25 IL–7
0.24 IL–4
0.23 IL–17F
0.2 IL–27
0.2 IL–6
0.16 Eotaxin
0.16 IL–23
0.08 IL–2
0.03 IL–12p70
0 IP–10
0 IFN–γ
0 IL–16
–0.02 MIP–1α
–0.04 IL–8
–0.04 Eotaxin–3
–0.05 IL–22
–0.07 IL–10
–0.09 TNF–β
–0.09 IL–12
–0.21 IL–1α
–0.24 IL–29
–0.34 IL–15
–0.36 IL–17A
–0.4 TNF–α
–0.48 IL–13
–0.54 IL–1β
E
quinolinic acid and MCP–1
T21
D21
Spearman correlation
D21: –0.57
T21: 0.56
MCP–1 (model residuals)
quinolinic acid (model residuals)
F
quinolinic acid and MCP–4
T21
D21
Spearman correlation
D21: –0.31
T21: 0.56
MCP–4 (model residuals)
quinolinic acid (model residuals)